PREDICTING LOWER STRATOSPHERIC WATER VAPOR FROM

CHEMISTRY-CLIMATE MODELS USING A MULTIVARIATE LINEAR

REGRESSION

A Thesis

by

KEVIN SMALLEY

Submitted to the Office of Graduate and Professional Studies of
Texas A&M University
in partial fulfillment of the requirements for the degree of

MASTER OF SCIENCE

Chair of Committee,   Andrew Dessler
Committee Members,   Kenneth Bowman
                     Gerald North
Head of Department,   Ping Yang

December 2016

Major Subject: Atmospheric Sciences

ABSTRACT

Climate models predict that tropical lower stratospheric humidity will increase as the climate warms, with important implications for the chemistry and climate of the atmosphere. We analyze this trend in 21st-century simulations from 12 state-of-the-art chemistry-climate models (CCMs) using a linear regression model to determine the factors driving the trends. The trend in humidity in the CCMs is driven by warming of the troposphere. This is partially offset in most CCMs by an increase in the strength of the Brewer-Dobson circulation, which tends to cool the tropopause layer. We also apply the regression model to individual decades from the 21st century CCM runs and compared them to the results from a regression of a decade of lower stratospheric humidity observations. Many of the CCMs, but not all, compare well with observations, lending credibility to their predictions. One notable deficiency in most CCMs is that they underestimate the impact of the quasi-biennial oscillation on lower stratospheric humidity. Our analysis provides a new way to evaluate model trends in lower stratospheric humidity.

ACKNOWLEDGMENTS

TABLE OF CONTENTS

Page

LIST OF FIGURES

LIST OF TABLES

1. INTRODUCTION

1.1 Motivation

Stratospheric water vapor plays a vital role in our atmosphere through many mechanisms. As a greenhouse gas, stratospheric water vapor warms the troposphere and cools the stratosphere [*Manabe and Wetherald*, 1967; *Maycock et al.*, 2014]. Stratospheric water vapor also impacts ozone concentrations [*Kirk-Davidoff et al.*, 1999; *Shindell*, 2001; *Stuber et al.*, 2001; *WMO*, 2007]. Simulations conducted by *Stenke and Grewe* [2005] show that long-term increases in stratospheric water vapor increase the persistence of polar stratospheric clouds during Antarctic spring and enhance ozone depletion. Additionally, stratospheric water vapor variations can affect tropospheric circulation. *Tandon et al.* [2011] found that cooling the stratosphere results in a poleward-shifted jet and an expanded yet weakened Hadley Cell, while *Maycock et al.* [2013] found that changes in stratospheric water vapor may shift storm tracks poleward. Therefore, understanding the processes responsible for changing stratospheric water vapor concentrations will improve our understanding of the climate system, and Chemistry-Climate Models (CCMs) provide us a mechanism to investigate this.

1.2 History of Study of Lower Stratospheric Water Vapor

Brewer [1949], using aircraft measurements obtained over England, found the stratosphere to be much dryer than the ambient temperature would imply. He thought this could be explained one of two ways: 1) by photochemical destruction of water vapor, or 2) by transport of air vertically through the cold tropical tropopause. Considering water vapor is photochemically destroyed in the upper atmosphere, Brewer correctly concluded that water vapor photolysis should not occur in the lower stratosphere. Thus, he concluded

1

that vertical advection through the tropical tropopause was the most logical explanation. As air transits this region, cold temperatures found there limit water vapor entering the stratosphere, and Brewer further hypothesized that this would be coupled with a slow overturning circulation featuring air rising through the tropical tropopause and then moving meridionally, poleward, and sinking at higher latitudes. *Dobson* [1956] reached similar conclusions using the ozone distribution, and this circulation has since became known as the Brewer-Dobson Circulation (BDC) (shown in Figure 1.1).
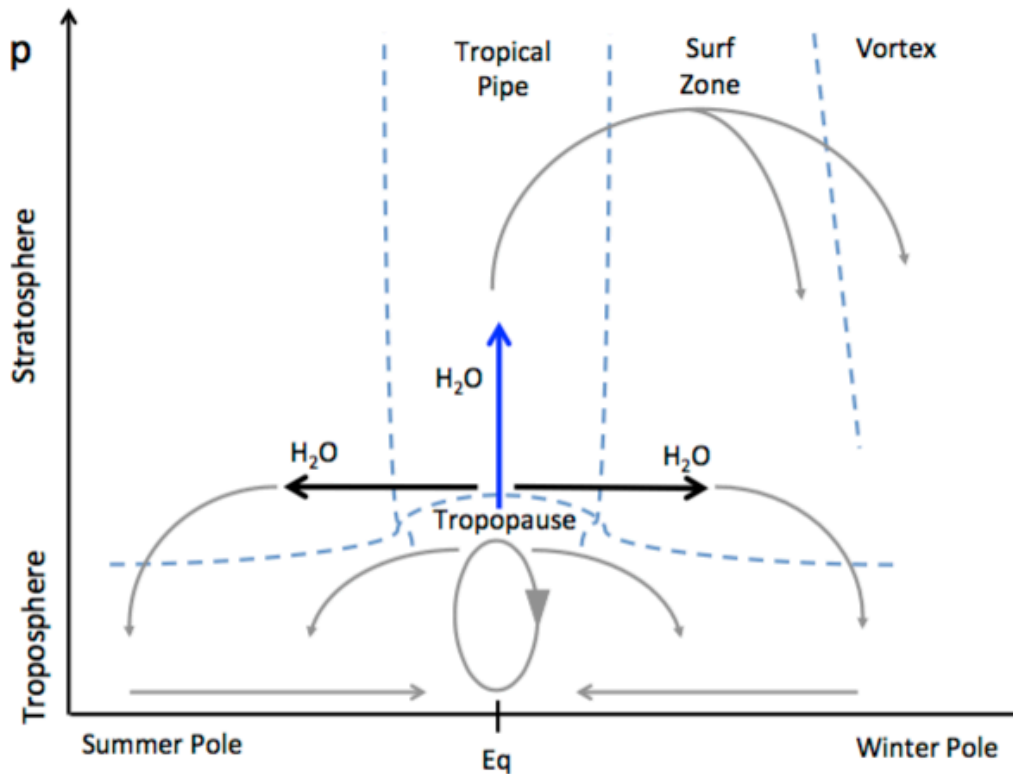
Figure 1.1: Adapted from *Flury et al.* [2013], this schematic represents the Brewer-Dobson Circulation. Air rises in the tropics crossing the tropopause, transporting trace gases into the lower stratosphere. From there, the Brewer-Dobson Circulation moves air meridionally until it sinks back towards the troposphere in the middle and upper latitudes.

Observations show only 3.2-4.8 ppmv remain after transport through the tropical tropopause, lower than many studies of the time expected [*Brewer*, 1949; *Mastenbrook*, 1968, 1971; *Kley et al.*, 1979; *Jones et al.*, 1986]. They questioned why observed water vapor mixing ratios in the lower stratosphere were so much smaller than expected. He concluded that there must be some sink not yet studied. To solve this, *Newell and Gould-Stewart* [1981] proposed that air crosses the tropical tropopause only at its coldest locations and at corresponding times of the year. According to this theory, a "stratospheric fountain" exists over the western tropical Pacific during northern hemisphere winter, and over the Bay of Bengal and India during monsoon. They postulated that this would explain stratospheric air being drier than expected, assuming a mean tropical tropopause temperature of -80° C.

However, problems do exist with the "stratospheric fountain" hypothesis [*Rosenlof*, 2003]. First, satellite data shows that air enters the stratosphere year round [*Mote et al.*, 1995], and is not restricted to certain times of the year. *Dessler* [1998] reviewed water vapor measurements and estimated a mixing ratio of 3.8 ppmv entering the stratosphere through the tropical tropopause, consistent with the average observed tropopause temperature. He concluded that because these observed mixing ratios are similar to expected values, the "stratospheric fountain" hypothesis is no longer necessary. Additionally, studies show that there may be net downward motion over the western Pacific contradicting the "stratospheric fountain" hypothesis [*Sherwood*, 2000; *Holton and Gettelman*, 2001].

If a "stratospheric fountain" is not responsible for regulating water vapor entering the lower stratosphere ($[H_2O]_{entry}$), what is? Temperature, wind, and tracer distributions show that, in the tropics, the tropopause is not a sharp boundary but a transition zone [*Sherwood and Dessler*, 2000; *Gettelman et al.*, 2002; *Fueglistaler et al.*, 2009a]. Called the tropical tropopause layer (TTL), it contains air with both tropospheric and stratospheric properties [*Sherwood et al.*, 2003], and acts as a "gate to the stratosphere" for atmospheric trace gases, including $[H_2O]_{entry}$ [*Fueglistaler et al.*, 2009a]. Found within the TTL is the

tropical cold-point tropopause (T_{cpt}). It represents the minimum temperature in the profile [*Gettelman and Fu*, 2002; *Fueglistaler et al.*, 2009a; *Kim and Son*, 2015] and is nearly coincident with the level of minimum water vapor saturation mixing ratios [*Sherwood and Dessler*, 2001; *Gettelman et al.*, 2002; *Fueglistaler et al.*, 2009a]. *Gettelman and Fu* [2002] investigated changes in the TTL during the recent past (1960-2000) and potential changes during the 21st century. One of their primary research questions was, how does a changing T_{cpt} effect $[H_2O]_{entry}$? They found that variations in cold-point temperature strongly effect $[H_2O]_{entry}$, consistent with *Gettelman et al.* [2002]. Several studies refer to the part of the TTL coinciding with the T_{cpt} as the "cold trap", and they find that tropical upwelling through the "cold trap" regulates water vapor entering the stratosphere to its minimum saturation vapor pressure [*Sherwood and Dessler*, 2000; *Holton and Gettelman*, 2001; *Fueglistaler and Haynes*, 2005; *Oman et al.*, 2008; *Garfinkel et al.*, 2013].

While Brewer's original hypothesis holds with a few caveats, important questions remain. For example, is $[H_2O]_{entry}$ increasing or decreasing? Previous studies have suggested that past $[H_2O]_{entry}$ has increased. For instance, using mean vapor pressure obtained by the UK frost-point hygrometer, *Roscoe and Rosenlof* [2011] concluded that from the 1950s until the 1970s, $[H_2O]_{entry}$ increased by $.08 \pm 0.03$ ppmv year^{-1}, with a total increase of 1 ppmv between the 1950s and 2010. *Hurst et al.* [2011] conducted a similar study analyzing observational (radiosonde data from Boulder Colorado) $[H_2O]_{entry}$ trends from 1980 until 2010. Overall, they found $[H_2O]_{entry}$ increased by 1.02 ± 0.24 ppmv during the entire period. Similar results were found by *Oltmans et al.* [2000] and *Rosenlof* [2003].

More recent studies cast doubt on this conclusion. *Hegglin et al.* [2014], using satellite data merged with CCM meteorology and nudged to observations to fill in gaps within the satellite data, examined stratospheric water vapor trends between the late 1980s and 2010. In the TTL, they found $[H_2O]_{entry}$ to decrease during this time-frame. They compared

their results to observations taken over Boulder CO cited by *Hurst et al.* [2011], and they conclude that the Boulder data-set should not be considered representative of the global stratosphere. *Dessler et al.* [2014], studying $[H_2O]_{entry}$ variations during the past 30 years, found similar results and cite little or no trend in $[H_2O]_{entry}$.

1.3 Processes Responsible for Stratospheric Water Vapor Variations

In the mid and upper stratosphere, water vapor is determined primarily by transport and methane oxidation [*Evans et al.*, 1998]. In the tropical lower stratosphere and at least on short time scales, $[H_2O]_{entry}$ exhibits a strong correlation with TTL temperatures [*Randel et al.*, 2006; *Rosenlof and Reid*, 2008; *Solomon et al.*, 2010]. Thus, to understand $[H_2O]_{entry}$ variations, processes responsible for TTL temperature modification need to be known. Fortunately, these processes are well documented and are discussed in subsequent sections. On longer time scales, however, the picture is fuzzier because we do not have good observational data sets. Models, however, suggest that long-term trends in convective injection of ice might drive trends in $[H_2O]_{entry}$ [*Dessler et al.*, 2016].

1.3.1 Brewer-Dobson Circulation

As discussed earlier, the BDC (Figure 1.1) is a slow overturning meridional circulation with an average tropical ascent rate of 0.2 mm sec^{-1} [*Flury et al.*, 2013], and first hypothesized by *Brewer* [1949] as an explanation of the aridity of the lower stratosphere. The BDC is driven by a slow down of zonal flow within the stratosphere by vertically propagating breaking planetary and gravity waves [*Haynes et al.*, 1991; *Holton et al.*, 1995; *Chen and Sun*, 2011; *Kim and Son*, 2015]. *Ueyama and Wallace* [2010] investigate what fraction of tropical upwelling can be attributed to breaking high-latitude waves and conclude that variability of high-latitude wave forcing affects the strength of tropical upwelling on interseasonal, annual, and interannual time scales. Additionally, *Geller and Zhou* [2008] postulates that the influence of wave drag on the interannual variability of tropical up-

welling could help explain interannual variability of observed stratospheric water vapor.

Previous studies have investigated how the BDC changes with climate. Focusing on climate change caused by anthropogenic forced warming, several studies show the BDC strengthens with increasing greenhouse gas emissions [*Randel et al.*, 2006; *Birner and Bönisch*, 2011; *Bönisch et al.*, 2011; *Ploeger et al.*, 2015]. *Randel et al.* [2006] concluded that anthropogenic forced warming sharpens the meridional temperature gradient. This increases wave propagation in the lower stratosphere strengthening the BDC, a result also found by *Li et al.* [2007]. *Castanheira et al.* [2012] found a significant anticorrelation exists between $[H_2O]_{entry}$ and tropical upwelling. One event illustrating this relationship is the significant drop in $[H_2O]_{entry}$ after 2001. *Randel et al.* [2006] concluded that a period of enhanced tropical upwelling resulted in colder TTL temperatures and subsequently less $[H_2O]_{entry}$. An abrupt drop in $[H_2O]_{entry}$ occured in 2011 for similar reasons [*Gilford et al.*, 2016]. Thus, strengthening the BDC by anthropogenic forced warming should reduce the humidity of parcels entering the tropical lower stratosphere. *Fueglistaler et al.* [2014] found, in response to increasing greenhouse gases, the TTL cools by approximatly 2 K per 10% change in upwelling, and corresponds to $[H_2O]_{entry}$ decreasing by 1 ppmv per 10% change in vertical ascent.

1.3.2 Quasi-Biennial Circulation

By analyzing monthly zonal wind components from 1955 until 1960, *Reed et al.* [1961] identified what would later become known as the Quasi-Biennial Oscillation (QBO) (shown in Figure 1.2). Zonal winds at the equator oscillate with a period of about two years between easterly and westerly. More importantly, the phase of the QBO impacts TTL temperature. The westerly phase of the QBO is associated with anomalously warm TTL temperatures, and the easterly phase is associated with anomalously cold TTL temperatures [*Zhou et al.*, 2001; *Geller et al.*, 2002]. As a result of the QBO's impact on

TTL temperatures, it also is important to the transport of trace gases, such as water vapor, into the stratosphere [*O'Sullivan and Dunkerton*, 1997; *Randel et al.*, 1998; *Dunkerton*, 1978; *Fueglistaler and Haynes*, 2005; *Choiu et al.*, 2006; *Liang et al.*, 2011; *Castanheira et al.*, 2012; *Khosrawi et al.*, 2013; *Kawatani et al.*, 2014; *Tao et al.*, 2015]. For instance, *Geller et al.* [2002] and *Kawatani et al.* [2014] investigated interannual variability of both MLS and climate model stratospheric water vapor. They found that the QBO dominates interannual variability of stratospheric water vapor with upward propagation of anomalies seen clearly from the lower to mid-stratosphere, and this propagation resembles the annual tape-recorder signal found in water vapor identified by *Mote et al.* [1996].
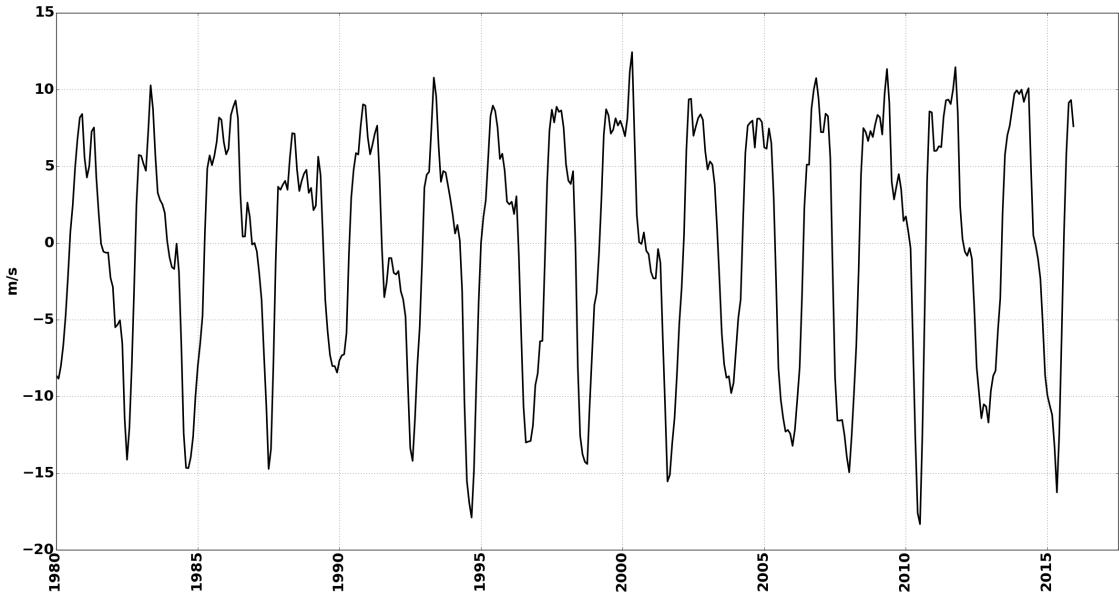
Figure 1.2: This plot shows the observed QBO downloaded from *CPC* [2016].

7

1.3.3 Tropospheric Temperatures

Climate models project the troposphere to warm by about $3°$ C during the 21st century [*Peters et al.*, 2013]. More water vapor can enter the lower stratosphere in one of two ways by warming the troposphere. First, a warming troposphere can simply radiatively heat the lower stratosphere warming the TTL and letting in more water vapor [*Gettelman et al.*, 2004]. The second way a warming troposphere can induce more water vapor into the lower stratosphere is by convection. A warmer climate results in a warmer boundary layer producing deeper and more energetic convection [*Chou and Chen*, 2010; *Posselt et al.*, 2012; *Sahany et al.*, 2014; *Tan et al.*, 2015; *an Chen et al.*, 2016]. Deep convection can penetrate the lower stratosphere [*Alcala and Dessler*, 2002; *Dessler*, 2002; *Rossow and Pearl*, 2007], and significantly affect characteristics of the TTL [*Dessler*, 2002; *Sherwood and Dessler*, 2003; *Jiang et al.*, 2004; *Riviere et al.*, 2006; *Russo et al.*, 2011]. *Paulik and Birner* [2012] point out a large-scale deep convective signal exists in TTL temperatures, and this signal can be broken into two effects, adiabatic and diabatic cooling [*Sherwood and Dessler*, 2001; *Read et al.*, 2008; *Jain et al.*, 2013]. As air rises inside a thunderstorm, deep convection rising into the TTL induces turbulent mixing, and adiabatic cooling [*Sherwood and Dessler*, 2001; *Read et al.*, 2008]. Diabatic cooling results from both cloud-top radiative cooling and sublimation of ice [*Sherwood and Dessler*, 2001; *Wu et al.*, 2005; *Hanisco et al.*, 2007; *Read et al.*, 2008; *Dessler et al.*, 2016].

Read et al. [2008] investigated three possible water vapor transport theories, slow uniform ascent across the TTL, hydrated overshooting convection (the mixing of water vapor that retains its ice into the TTL), and convective mixing (the mixing of water vapor without the retention of ice). Both slow ascent and overshooting convection advect water vapor into the stratosphere, while convective mixing acts as a dehydration mechanism. In regards to overshooting convection, lofted ice has become a popular study topic because ice in-

jected into the stratosphere by deep convection can sublimate or evaporate, hydrating the lower stratosphere [*Moyer et al.*, 1996; *Keith*, 2000; *Johnson et al.*, 2001; *Kuang et al.*, 2003; *Wu et al.*, 2005; *Hanisco et al.*, 2007; *Corti et al.*, 2008; *Read et al.*, 2008; *Khaykin et al.*, 2009; *Ueyama et al.*, 2015; *Dessler et al.*, 2016].

1.3.4 Volcanic Eruptions

Large volcanic eruptions can inject aerosols into the stratosphere. These aerosols change the temperature and dynamics of the TTL and lower stratosphere [*Joshi and Jones*, 2009; *Arfeuille et al.*, 2013]. *Löffler et al.* [2016] investigated stratospheric water vapor perturbations generated by the El Chichon and Mt. Pinatubo eruptions using the ECHAM/MESSy Atmospheric Chemistry (EMAC) model. Volcanic aerosols injected near the equator radiatively heat the lower stratosphere., and they found that this warming resulted in an increase of 0.3 ppmv of water vapor at around 90 hPa shortly after each eruption. Induced warming began to cool back to pre-eruption values within approximately two years. *Dessler et al.* [2014], analyzing processes varying observed $[H_2O]_{entry}$, found similar results concluding that volcanic eruptions add $[H_2O]_{entry}$ to the lower stratosphere as a result of warming the TTL.

1.4 Climate Models

Global Climate Models (GCMs) can help predict and understand future climate change. GCMs have limited ability to simulate the TTL and stratosphere, so to understand those regions we turn to models specifically designed to simulate those regions. These Chemistry Climate Models (CCMs) have been widely used by the community for these research questions [*SPARC*, 2010; *Morgenstern et al.*, 2010; *Eyring et al.*, 2013].

Before you can believe predictions of the CCMs, however, it is imperative that we use observations to validate the models [*Austin et al.*, 2003]. *Gettelman et al.* [2010] developed a grading method to quantitatively evaluate the performance of 18 CCMs in reproducing

9

characteristics of the TTL. For our purpose, we highlight two of their diagnostics (T_{cpt} and $[H_2O]_{entry}$). Because T_{cpt} is the primary mechanism regulating $[H_2O]_{entry}$ that enters the stratosphere [*Brewer*, 1949; *Gettelman and Fu*, 2002; *Fueglistaler et al.*, 2009a], do CCMs accurately simulate the T_{cpt}? *Gettelman et al.* [2010] finds that most models reproduce both amplitude and timing of its annual cycle in comparison to observations. It would seem plausible that the annual cycle of $[H_2O]_{entry}$, in turn, is also realistically simulated. However, the annual cycle of $[H_2O]_{entry}$ is not well reproduced, with the annual cycle shifted by 1-2 months in comparison to observations from the Halogen Occultation Experiment (HALOE) [*Gettelman et al.*, 2010].

Using CCMs, previous studies not only investigate trends, both historical and future, in $[H_2O]_{entry}$, but also to examine physical processes responsible for $[H_2O]_{entry}$ variability. For instance, *Austin et al.* [2007] found $[H_2O]_{entry}$ from 1960-2000 increased during a period of enhanced upwelling. Using coupled CCM simulations; In the mid and upper stratosphere, *Oman et al.* [2008] found stratospheric water vapor increased between 1950 and 2000 due to changes in methane concentrations, while, in the lower stratosphere, $[H_2O]_{entry}$ decreased during the same time-frame. *Hardiman et al.* [2015] found, from CMIP5 GCMs, that microphysical and radiative processes influence $[H_2O]_{entry}$ by modifying T_{cpt} and upper-tropospheric water vapor concentrations. Most studies conclude that long-term increases in $[H_2O]_{entry}$ coincide with warming the TTL [*Fueglistaler and Haynes*, 2005; *Oman et al.*, 2008; *Gettelman et al.*, 2009; *Garfinkel et al.*, 2013]. However, *Dessler et al.* [2016] found that lofted ice, in addition to TTL warming, accounts for a significant portion of the positive long-term trend in $[H_2O]_{entry}$ simulated by CCMs.

1.5 Thesis Goals

The main goal of this study is to test water vapor variability in an ensemble of CCMs. Our goals are to use multivariate linear regressions to understand short- and long-term

$[H_2O]_{entry}$ variability using a few key processes as predictors (Tropospheric warming (ΔT), the BDC, and the QBO).

2. MODELS AND METHODOLOGY

2.1 Model Data

We analyze model output from 7 CCMs participating in Phase 2 of the Chemistry-Climate Model Validation Project (CCMVal-2) (*Morgenstern et al.* [2010]; *SPARC* [2010]; shown in Table 2.1) and output from 5 CCMs participating in Phase 1 of the Chemistry-Climate Model Initiative (CCMI-1) (*Eyring et al.* [2013]; shown in Table 2.1). These CCMs were developed to model stratospheric chemical and dynamical processes.

We investigate simulations from the REF-B2 scenario in CCMVal-2, and the refC2 scenario in CCMI-1, which include anthropogenic forcings that drive a changing climate in both scenarios. Greenhouse gas concentrations are initialized using observations, while post-2000 greenhouse gas concentrations come from the A1B scenario, which lies in the middle of the SRES scenarios [*IPCC*, 2001]. Ozone-depleting substances come from the halogen emission scenario A1, which features a decline of halogen emissions during the 21st century [*WMO*, 2007]. For CCMVal-2, model specifics can be found in both *SPARC* [2010] and *Morgenstern et al.* [2010], while CCMI-1 model specifics can be found in *Eyring et al.* [2013].

We are concerned with $[H_2O]_{entry}$ variations during the 21st century. Ideally, model data would be available throughout the entire 21st century ranging from 2000-2100, however several model simulations end a few years prior to 2100. In order to maintain a consistent reference-period between models, our analysis covers 2000-2097, which we will refer to for convenience as "the 21st century".

2.2 Model Variables

In this study, we analyze tropical (30 north - 30 south; see Figure 2.1) averages of lower stratospheric water vapor and the BDC at 80 hPa, tropical tropospheric temperature

variations at 500 hPa, and a 50-hPa QBO index. To tropically average the data, we, zonally average each global CCM variable and, we meridionally average the data between 30 north and 30 south, weighting it by cosine of latitude. We assume, here, that 80-hPa water vapor volume mixing ratios is a proxy for $[H_2O]_{entry}$, and we use lower stratospheric diabatic vertical velocities derived from 80-hPa radiative heating (see *Fueglistaler et al.* [2009b] for details) as a proxy for BDC strength.
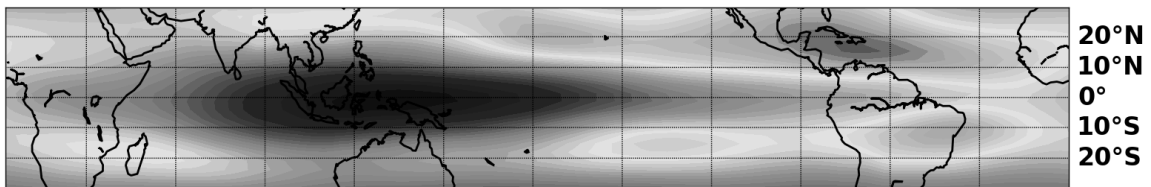
Figure 2.1: This plot shows MRI climatological 80-hPa water vapor (1960-2100) confined between (30 north and 30 south), which we define as the tropics.

Not all CCMs simulate a QBO (*SPARC* [2010]; *Morgenstern et al.* [2010]; *Eyring et al.* [2013]; shown in table 2.1). To verifiy this, we calculate a QBO index for each CCM. We accomplish this by plotting 50-hPa zonal winds and standardized them by the time-series standard deviation. Then, we look for an oscillation about zero with a period of about 28 months [*Anstey et al.*, 2016]. For instance, Figure 2.2 verifies that MRI simulates a realistic QBO, additionally we find that CCSRNIES-MIROC3.2, CMAM-CCMI, GEOSCCM-CCMI, MRI-ESM1r1, and NIWA-UKC (all not shown) realistically simulate a QBO.
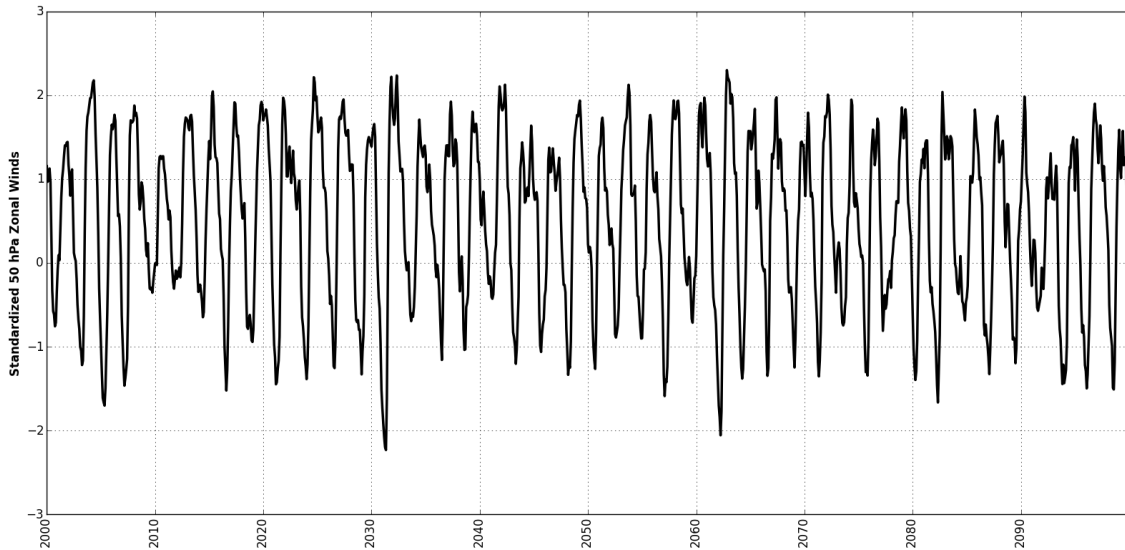
Figure 2.2: This plot shows the 50-hPa QBO Index simulated by the MRI between 2000 and 2100. We calculate the QBO index by standardizing MRI zonal winds at the equator by the time-series standard deviation.

Typically, among CCMs that realistically simulate a QBO, correlation between $[H_2O]_{entry}$

14

the 50-hPa QBO index is small, generally less than 0.25. This possibly indicates that the relationship between $[H_2O]_{entry}$ and the QBO index at this pressure level is small. We still use 50-hPa zonal winds instead of a level with a stronger correlation to $[H_2O]_{entry}$, because *CPC* [2016] archives the QBO index at both 30 and 50 hPa, and we want to compare CCM results to observations, which we will discuss in chapter 4.

All CCMVal-2 and most CCMI data is given on isobaric surfaces, however a few CCMI-1 simulations only produce variables on hybrid pressure levels (CMAM, CCSRNIES-MIROC3.2, and MRI-ESM1r1). In the stratosphere, hybrid pressure levels are nearly isobaric and do not pose much of an issue, but in the troposphere hybrid pressure levels are not isobaric and can deviate from an isobaric surface [*Kulyamin and Dymnikov*, 2014]. For these models, we choose a hybrid pressure level close to the 500-hPa pressure surface (See Table 2.1).

Table 2.1: Details about each CCM. The resolution is listed as (lat x lon x number of pressure levels). 31 vertical levels indicates CCM data is given on isobaric levels, while CCMs simulating data on >31 levels are given on sigma (hybrid-pressure) levels

Chemistry Climte Model Properties				
CCM	Resolution	Dataset	Contains QBO	Institution
CCSRNIES	2.8° x 2.8° x 31	CCMVal-2	No	NIES, Tsukuba, Japan
CCSRNIES-MIROC3.2	2.8° x 2.8° x 34	CCMI-1	Yes	NIES, Tsukuba, Japan
CMAM	5.5° x 5.6° x 31	CCMVal-2	No	EC, Canada
CMAM-CCMI	3.7° x 3.8° x 71	CCMI-1	Yes	EC, Canada
CNRM-CM5-3	2.8° x 2.8° x 31	CCMI-1	Yes	Meteo-France; France
GEOSCCM	2.0° x 2.5° x 31	CCMVal-2	No	NASA/GSFC, USA
GEOSCCM-CCMI	2.0° x 2.5° x 72	CCMI-1	Yes	NASA/GSFC, USA
LMDZrepro	2.5° x 3.8° x 31	CCMVal-2	No	IPSL, France
MRI	2.8° x 2.8° x 31	CCMVal-2	Yes	MRI, Japan
MRI-ESM1r1	2.8° x 2.8° x 80	CCMI-1	Yes	MRI, Japan
NIWA-UKCA	2.5° x 3.8° x 31	CCMI-1	Yes	NIWA, NZ
WACCM	1.9° x 2.5° x 31	CCMVal-2	No	NCAR, USA

2.3 Methodology

To analyze $[H_2O]_{entry}$, we use a multivariate linear regression (MLR). This type of analysis has long been used in atmospheric science, especially to analyze stratospheric constituents. For instance, *Poulain et al.* [2016] analyzed variability of several lower stratospheric trace gases simulated by CCMs including: O_3, HCl, NO_2, and N_2O. Focusing on O_3, several studies have utilized MLR analysis to quantify both O_3 loss due to anthropogenic activity [*WMO*, 1998, 2007, 2011], and O_3 variability [*Hood and McCormack*, 1992; *Bodeker et al.*, 2001; *Reinsel et al.*, 2002; *Svendby and Dahlback*, 2004; *Brunner et al.*, 2006; *Dhomse et al.*, 2006; *Wohltmann et al.*, 2007; *Randel and Wu*, 2007; *Wohltmann et al.*, 2008]. Not many studies have used this methodology to investigate $[H_2O]_{entry}$ variability. *Schieferdecker et al.* [2015] utilized MLR methodology to investigate if a solar signal signal exists in $[H_2O]_{entry}$. While, *Dessler et al.* [2013, 2014] investigate whether or not $[H_2O]_{entry}$ can be fit using a MLR through a discrete set of "explanatory" variables (ΔT, BDC, and QBO), which our study follows closely.

As its name implies, a MLR is a linear function, and this function can be described by Equation 2.1.

$$\hat{y} = \sum_{n=o}^{N} \hat{\beta}_n x_n + \epsilon \tag{2.1}$$

$\hat{y}$ represents an estimate of the variable one may want to reconstruct or predict (i.e. predictor), and the variables used to predict $\hat{y}$ is a set of explanatory variables ($x_0, x_1, x_2, ..., x_n$). Ideally, explanatory variables evaluated are orthogonal to each other (little correlation with each other), but are correlated with $\hat{y}$ [*Pearce and Reiter*, 1985; *Jaccard et al.*, 1990; *Montgomery and Peck*, 1992a; *Marrow-Howell*, 1994]. As pointed out by *Pearce and Reiter* [1985], a high-degree of correlation between explanatory variables (multicollinearity) lessens the precision of each MLR estimate. Each $\hat{\beta}_n$ (except the y-intercept term $\hat{\beta}_0$) represents the slope term associated with each explanatory variable, and each is esti-

mated using least-squares (this process is explained thoroughly in [*Montgomery and Peck*, 1992b]. ϵ represents the amount of error associated with a MLR. Specifically, it represents the residual values $(y - \hat{y})$ between the estimated predictor estimated by MLR analysis and the actual predictor variable (y).

The coefficient of determination (R^2) has been long established as one of the primary statistics used to measure goodness-of-fit of a regression [*Montgomery and Peck*, 1992b]. Formally, R^2 is a measure of the amount of variance explained by regression analysis and ranges between 0 and 1. R^2 always increases as the number of predictor variables increase [*Montgomery and Peck*, 1992b]. To account for this artificial inflation of R^2 values, and prevent overfitting the data being modeled, R^2 is scaled by the number of predictors to give a more realistic goodness-of-fit value (hereby adjusted R^2).

In this study, we attempt to model CCM $[H_2O]_{entry}$ using a MLR with ΔT, the BDC, and the QBO as explanatory variables. These variables and how they interact with $[H_2O]_{entry}$ are discussed in chapter 1, and specifics of the regression equations we examine are given in chapters 4 and 5.

For each β term included in this study we calculate a 95% confidence interval to account for model uncertainties. However, we are dealing with time-series data. This potentially introduces problems into our regression. As explained prior, one primary assumption of a MLR is independent residuals. Obviously, residuals correlated with residuals at prior time-steps violates this assumption. We account for this issue by reducing the number of independent observations (degrees of freedom) using an estimated lag-1 autocorrelation of the residuals, as explained by *Santer et al.* [2000], and typically reducing the number of degrees of freedom from 100 years to on average 62 years (table 2.2). We then use the reduced degrees of freedom to calculate β uncertainties, expecting CCMs such as CMAM-CCMI and NIWA-UKCA with the lowest degrees of freedom, or the highest lag-1 autocorrelation, to produce the widest confidence intervals.

Table 2.2: This table lists the total number of independent observations (degrees of freedom) of the 21st century regressions.

CCM Independent Observations for the 21st Century Dataset	
CCM	degrees of freedom (years)
CCSRNIES	75
CCSRNIES-MIROC3.2	40
CMAM	55
CMAM-CCMI	30
CNRM-CM5-3	34
GEOSCCM	90
GEOSCCM-CCMI	79
LMDZrepro	91
MRI	96
MRI-ESM1r1	56
NIWA-UKCA	31
WACCM	70
average	62

3. CENTURY REGRESSIONS

3.1 Why Century Regressions?

As discussed previously, $[H_2O]_{entry}$ plays a vital role in our climate system. Previous studies find they can fit observational $[H_2O]_{entry}$ using a MLR with a strong statistical fit [*Dessler et al.*, 2013, 2014]. Can we fit 21st century $[H_2O]_{entry}$ simulated by CCMs? In addition to investigating observational $[H_2O]_{entry}$, *Dessler et al.* [2013] used the same methodology to analyze 21st century $[H_2O]_{entry}$ simulated by GEOSCCM. They found MLR analysis accurately reproduces GEOSCCM $[H_2O]_{entry}$ (see Figure 3.1). We test in this analysis whether other models behave similarly.
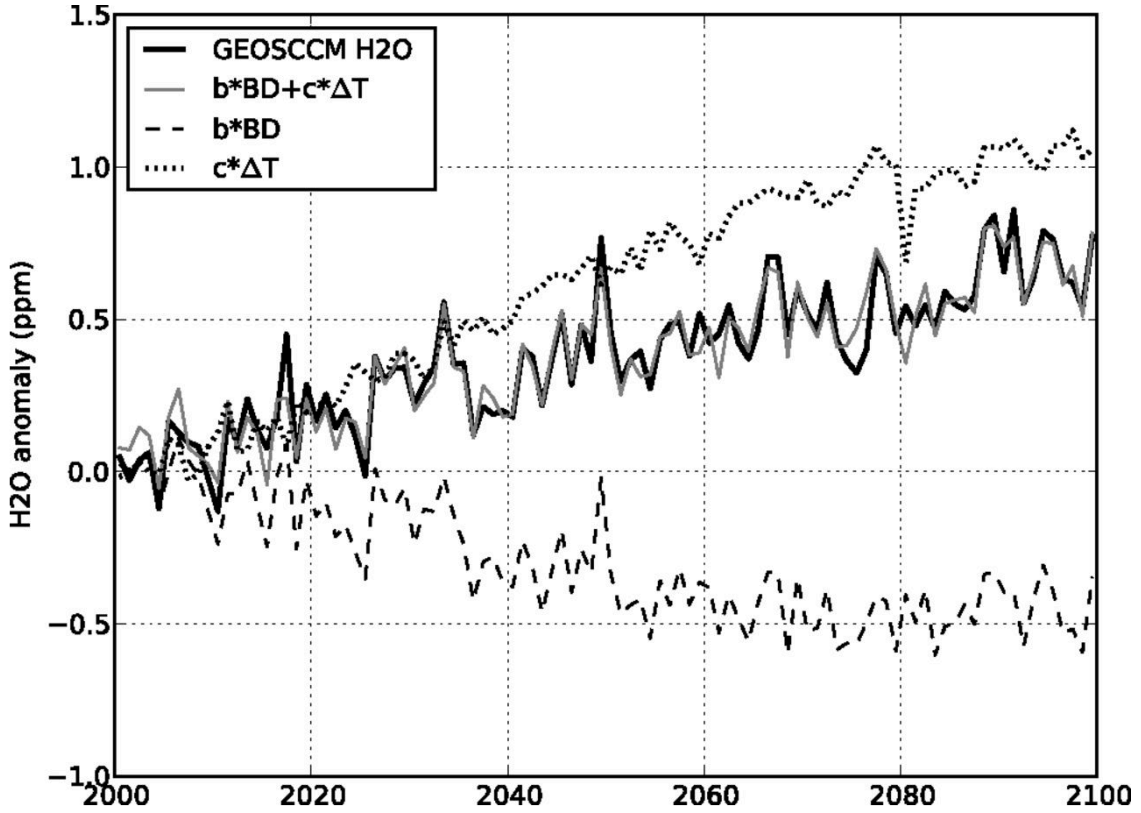
Figure 3.1: Adapted from *Dessler et al.* [2013], 21st century annual anomalies of $[H_2O]_{entry}$ from the GEOSCCM (black), and it is reconstructed using a MLR (gray) with ΔT (dotted) and BDC (dashed) annual anomalies as predictor variables.

3.2 Century Regression Equation

We analyze 21st century tropically averaged annual $[H_2O]_{entry}$ anomalies, calculated by subtracting off the reference-period (2000-2097) average from annually averaged values, using MLR methodology (hereby century MLR; Equation 3.1).

$$[H_2O]_{entry} = \beta_0 + \beta_{\Delta T}\Delta T + \beta_{BDC}\Delta BDC + \epsilon \tag{3.1}$$

$[H_2O]_{entry}$ is regressed against a set of physical processes identified in 2.2. We initially included a QBO term in the century MLR analysis. However, after analyzing the results, we found that including the QBO does not significantly improve the century MLRs, thus we omit the QBO. Investigating the individual slope terms in equation 3.1: β_0 represents the y-intercept term. $\beta_{\Delta T}$ corresponds to the gain or loss of $[H_2O]_{entry}$ due to changes in tropical tropospheric temperatures in ppmv K^{-1}, while β_{BDC} measures $[H_2O]_{entry}$ variance as a result in changes in the BDC in ppmv K^{-1} Day^{-1}. Finally, residual errors between actual CCM $[H_2O]_{entry}$ and MLR $[H_2O]_{entry}$ (MLR $[H_2O]_{entry}$ - CCM $[H_2O]_{entry}$) corresponds to ϵ.

For example, Figure 3.2 shows MRI $[H_2O]_{entry}$ increases by about 1.5 ppmv during the 21st century. A similar trend is reconstructed by the MRI century MLR. Investigating other simulations, (shown in Appendix A), we find all CCMs simulate $[H_2O]_{entry}$ increasing throughout the 21st century, and corresponding century MLRs are able to accurately reconstruct the long-term trends in simulated $[H_2O]_{entry}$.
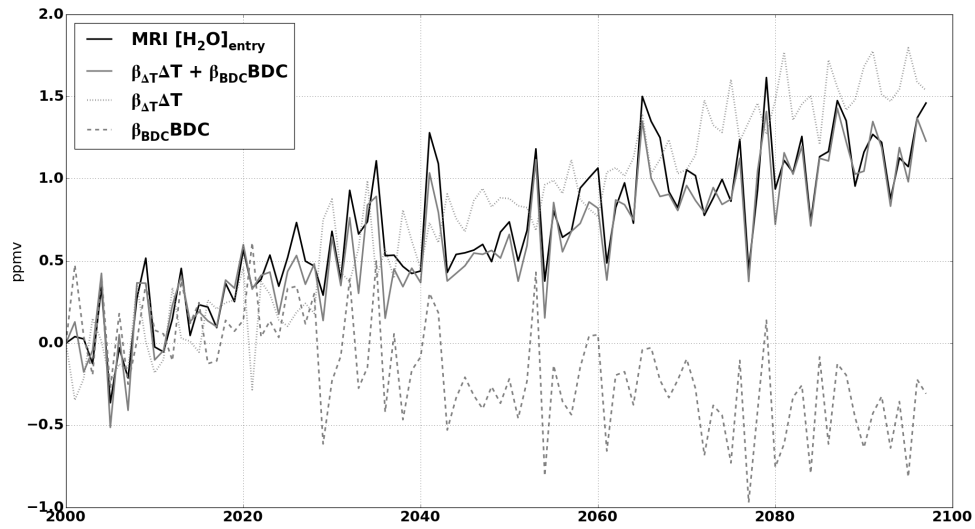
Figure 3.2: 21st century annual anomalies of $[H_2O]_{entry}$ from the MRI (black), and it reconstructed by a multivariate linear regression (gray) using ΔT (dotted) and BDC (dashed) annual anomalies as predictor variables.

As expected, Figure 3.3 shows all CCM century MLRs generate large adjusted R^2 values between 0.8 and 0.9±0.1. The NIWA-UKCA century MLR (shown in Appendix A) adjusted R^2 value represents the only outlier with a value of approximately 0.6. Adjusted R^2 values >0.6 are typically seen as valid indicators of a strong regression fit to actual data. However, long-term trends exist in all variables. Even if no relationship exists between a predictor and the explanatory variable estimated by a MLR, long-term trends bias adjusted R^2 values towards values closer to 1. Thus, additional analysis is needed.
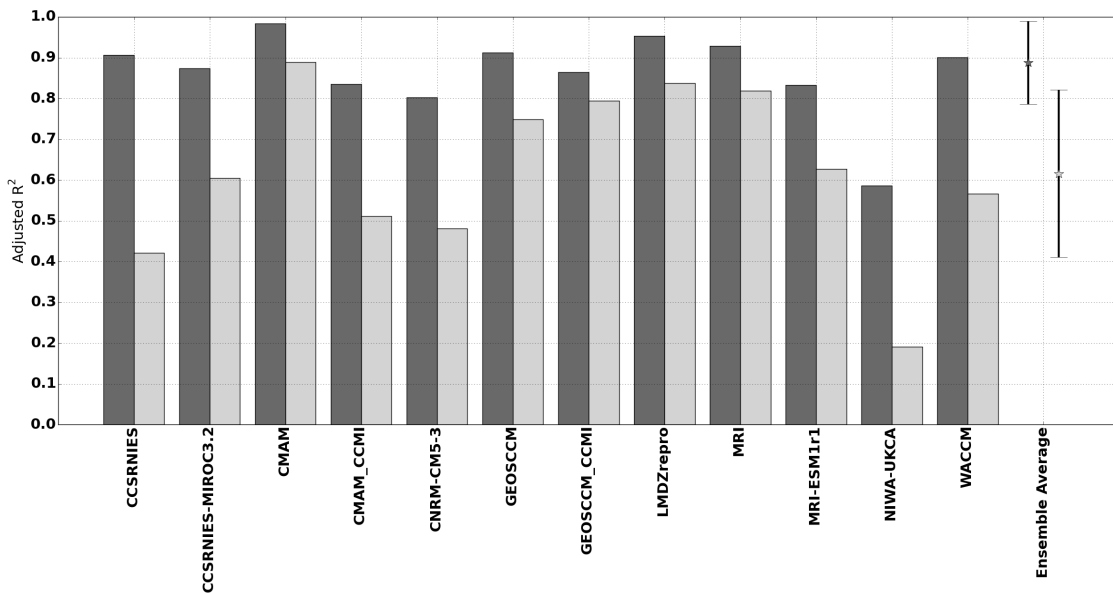
Figure 3.3: Each bar corresponds to both trended (dark grey) and detrended (light grey) adjusted R^2 values. The dark grey star represents the CCM ensemble mean trended adjusted R^2 value, while the light grey star represents to the CCM ensemble mean detrended adjusted R^2 value. Error bars, for both ensemble means, corresponds to the standard deviation of all CCM century (trended and detrended) adjusted R^2 values.

3.3 Detrended Variables

To eliminate the influence of long-term trends on adjusted R^2, we detrend each variable and analyze effectiveness of the MLR in capturing the short-term (interannual) variability in $[H_2O]_{entry}$. We accomplish this by applying a fast fourier transform (fft) to each variable [*Donnelly*, 2006], removing signals in each variable corresponding to periods ¿ 10 years (shown in Figure 3.4), and applying an inverse fft to obtain the detrended time series of each variable. We then regress the detrended $[H_2O]_{entry}$ against detrended ΔT and BDC. We now can test each MLR's ability in capturing $[H_2O]_{entry}$ interannual variability.
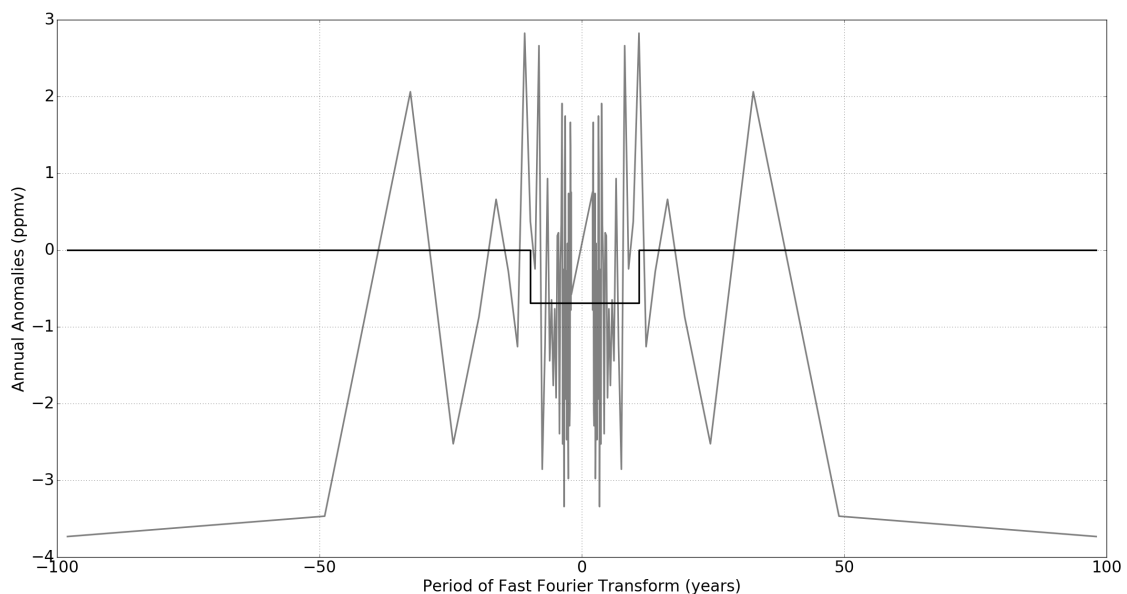
Figure 3.4: This plot shows signals in the annual anomalies of MRI $[H_2O]_{entry}$ (gray) produced using a fft. To detrend $[H_2O]_{entry}$. As represented by the square wave (black; average $[H_2O]_{entry}$ signal constrained to [-10,10] years), signals corresponding to fft periods ¿ 10 years are removed.

Reviewing Figure 3.3, we see that large differences exist between the unfiltered (previously

century MLR, now trended MLR) and detrended adjusted R^2 values for certain CCMs. For instance, the CCSRNIES trended century MLR captures approximately 90% of the variance in $[H_2O]_{entry}$, while the detrended century MLR only explains about 40% of interannual variance; similar patterns exist in CMAM-CCMI, CNRM-CM5-3, and NIWA-UKCA. As discussed previously, long-term trends skew adjusted R^2 values. Thus, to identify MLRs accurately reconstructing $[H_2O]_{entry}$ interannual variability, we look for small differences between both adjusted R^2 values, or large detrended adjusted R^2 values.

Examining results from the MRI, Figure 3.5 shows that the detrended MLR looks very similar to detrended $[H_2O]_{entry}$. Figure 3.3 confirms this, showing MRI's detrended MLR analysis producing an adjusted R^2 value of approximately 0.83. For MRI, the linear statistical model accurately reproduces interannual variability of $[H_2O]_{entry}$. Looking at the model ensemble average detrended adjusted R^2 value, most CCMs effectively reproduce $[H_2O]_{entry}$ interannual variability as indicated by detrended adjusted R^2 values > 0.7. In particular, CMAM, LMDZrepro, and (previously discussed) MRI perform exceptionally well, explaining $> 80\%$ of $[H_2O]_{entry}$ interannual variability.
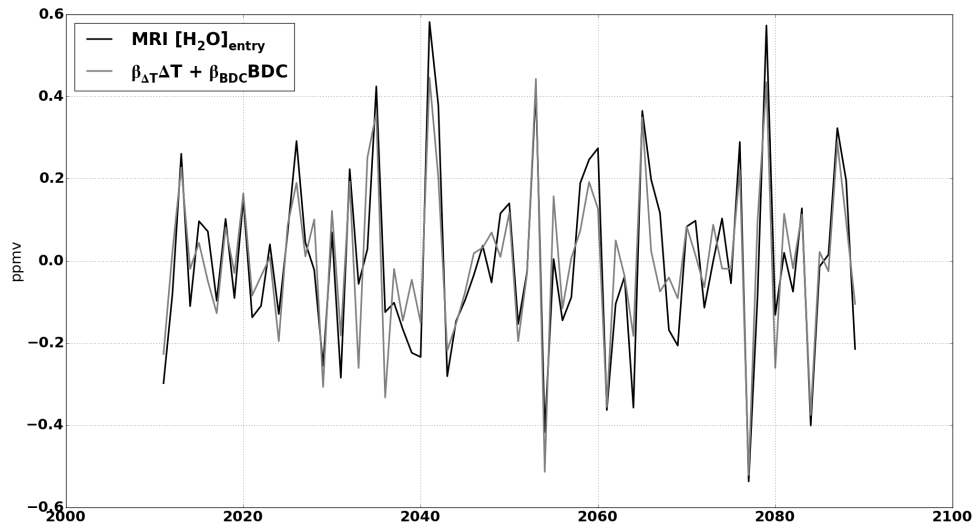
Figure 3.5: 21st century annual anomalies of detrended $[H_2O]_{entry}$ from the MRI (black), and it is reconstructed by a multivariate linear regression (gray) using ΔT and BDC (both not shown) annual anomalies as predictors. For this plot, all variables have been detrended by filtering long-term >10 years variations out.

3.4 Physical Process Effects

MLR analysis provides an excellent pathway to understanding how each predictor variable affects the regression. Investigating the sign and magnitude of each slope term, β_1 (ΔT regression coefficient) and β_2 (BDC regression coefficient), gives us the relationship between each process and $[H_2O]_{entry}$. For MRI, $[H_2O]_{entry}$ increases by about 1.5 ppmv during the 21st century. Figure 3.2 shows that ΔT accounts for the $[H_2O]_{entry}$ increase, while a strengthening BDC reduces $[H_2O]_{entry}$ entering the stratosphere by approximately 0.25 ppmv. Now that we know the effect of each process on MRI $[H_2O]_{entry}$, the next questions that we must answer for all CCMs are: 1) How does $[H_2O]_{entry}$ change as each process changes? and 2) Why does $[H_2O]_{entry}$ increase or decrease as a result of changing each process?
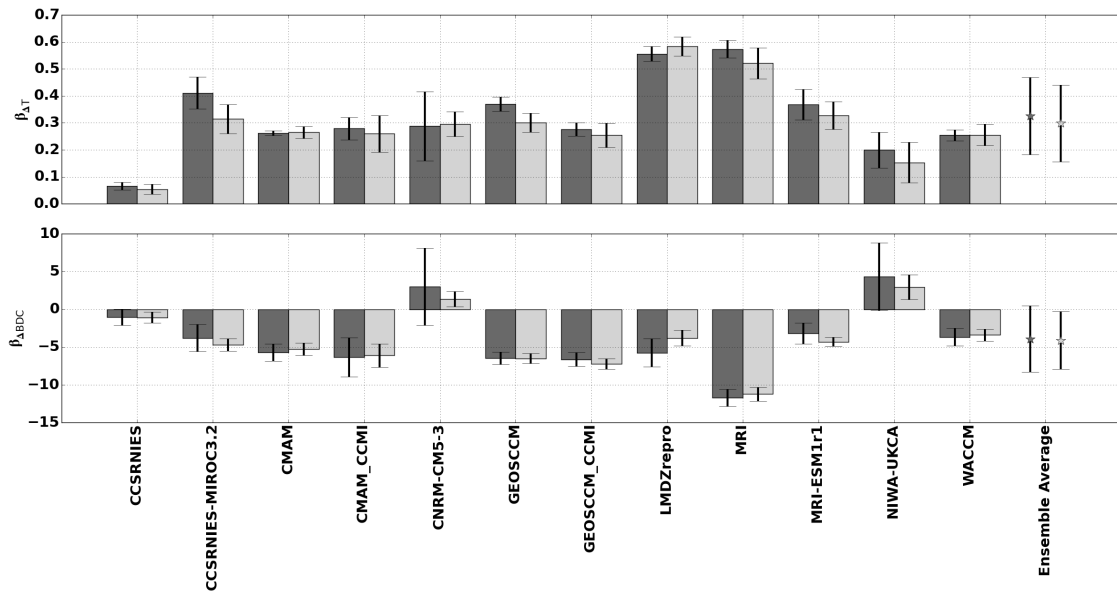
Figure 3.6: This plot shows the magnitude of each century regression coefficient (trended (dark grey) and detrended (light grey)), and error bars corresponding to each bar references the uncertainty (95th percentile confidence interval) in the regression coefficients. Each ⋆ represents the CCM ensemble average century regression coefficients (trended (dark grey) and detrended (light grey)), and corresponding error bars represent the variability (±standard deviation) in all CCM century regression coefficients

3.4.1 Tropospheric Warming

For all CCMs, Figure 3.6 shows that $[H_2O]_{entry}$ increases as ΔT increases. Additionally, the ΔT regression coefficients corresponding to trended and detrended MLRs are similar in sign and within a factor of 2. This indicates that ΔT affects both $[H_2O]_{entry}$ trended and detrended variability similarly. On average, $[H_2O]_{entry}$ increases by about 0.3 ± 0.1 ppmv K^{-1}. LMDZrepro and MRI century MLRs generate the largest ΔT regression coefficients, approximately 0.5 ppmv K^{-1}, while the CCSRNIES century MLR produces the smallest ΔT regression coefficients, approximately 0.1 ppmv K^{-1}. For all other CCMs, the ΔT regression coefficient does not deviate far from the model average ΔT regression coefficient. Thus, the CCMs all predict that a warming climate increases $[H_2O]_{entry}$ in the lower stratosphere.

3.4.2 Brewer-Dobson Strength

Figure 3.6 shows that the BDC reduces $[H_2O]_{entry}$ in all CCMs except CNRM-CM5-3 and NIWA-UKCA . As shown for ΔT, BDC regression coefficients for century MLRs (both detrended and trended) are similar in sign and magnitude suggesting that both have a similar effect on $[H_2O]_{entry}$. In general, the BDC regression coefficient is responsible for a decrease of 5 ± 1 ppmv $(K/Day)^{-1}$. The MRI's BDC regression coefficient accounts for a reduction of about 12 ppmv $(K/Day)^{-1}$, larger than BDC regression coefficients from all other models. As mentioned previously, the BDC coefficient produced by both the CNRM-CM5-3 and NIWA-UKCA is positive, which is contrary to our expectations of a strong BDC cooling the TTL. Overall, though, we find a strengthening BDC results in less $[H_2O]_{entry}$ advected through the TTL into the lower stratosphere in the CCMs. From Figure 3.7, we see that large detrended BDC regression coefficients typically correspond to large detrended adjusted R^2 values, and CCM detrended MLRs producing the smallest in magnitude BDC regression coefficients typically perform the poorest. In particular,

CCSRNIES, CNRM-CM5-3, and NIWA-UKCA generate some of the smallest BDC regression coefficients of any CCM, and they subsequently reproduce $[H_2O]_{entry}$ the poorest with detrended adjusted R^2 values <0.5.
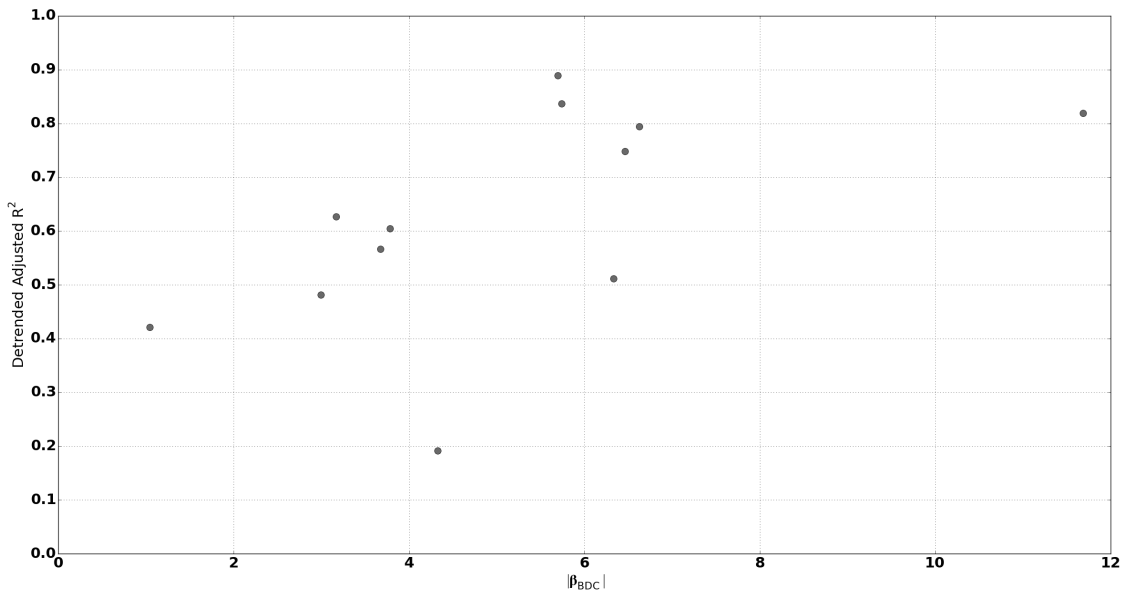
Figure 3.7: Scatter plot of CCM detrended BDC regression coefficients (ppmv $(K/Day)^{-1}$), vs. detrended adjusted R^2 values.

3.5 Physical Process Relative Magnitude

Because each regression coefficient has different units, we cannot directly compare relative magnitude of each coefficient in order to determine which one is more important. To address this, we standardize each time-series by its standard deviation and rerun each century MLR (hereby standardized century MLR). This effectively creates unitless variables and regression coefficients allowing us to compare the relative magnitude of each coefficient.
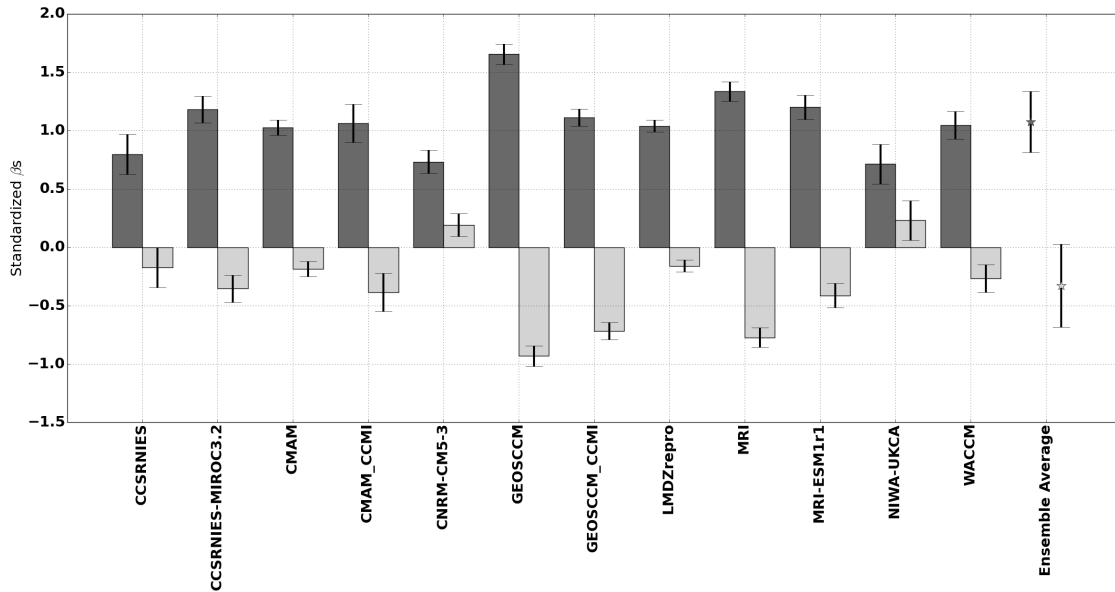
Figure 3.8: Each set of bars corresponds to the trended regression coefficients ($\beta_{\Delta T}$ (dark grey) and β_{BDC} (light grey)) produced by MLR analysis after standardizing each variable (ΔT and BDC) by dividing out the time-series (2000-2097) $\pm$standard deviation, and error bars corresponding to each bar represents the uncertainty of each coefficient as the 95th percentile confidence interval. Trended CCM ensemble average values for $\beta_{\Delta T}$ (dark grey) and β_{BDC} (light grey) are both represented by a $\star$, and corresponding error bars show variability (as the $\pm$standard deviation) in all CCM standardized regression coefficients.

From Figure 3.8, we see that ΔT effects $[H_2O]_{entry}$ more than the BDC. Standardized ΔT regression coefficients average 0.7 ± 0.1, and are generally similar in magnitude between all CCMs. The GEOSCCM standardized ΔT regression coefficient is an outlier in comparison to all other CCMs with a value of <1.5. While, standardized BDC regression coefficients are generally small averaging $-0.3/pm0.1$, and are much smaller than their ΔT counter parts. However, the GEOSCCM, GEOSCCM-CCMI, and MRI standardized BDC regression coefficients are much larger than those from all other models >0.7. Additionally, both standardized regression coefficients from the GEOSCCM, GEOSCCM-CCMI, and MRI are much closer in magnitude than those from the other CCMs. Thus, Figure 3.8

quantifies what we already know by looking at the time-series plot of each regression component, in that ΔT increases $[H_2O]_{entry}$ to a much larger degree than the BDC decreases $[H_2O]_{entry}$.
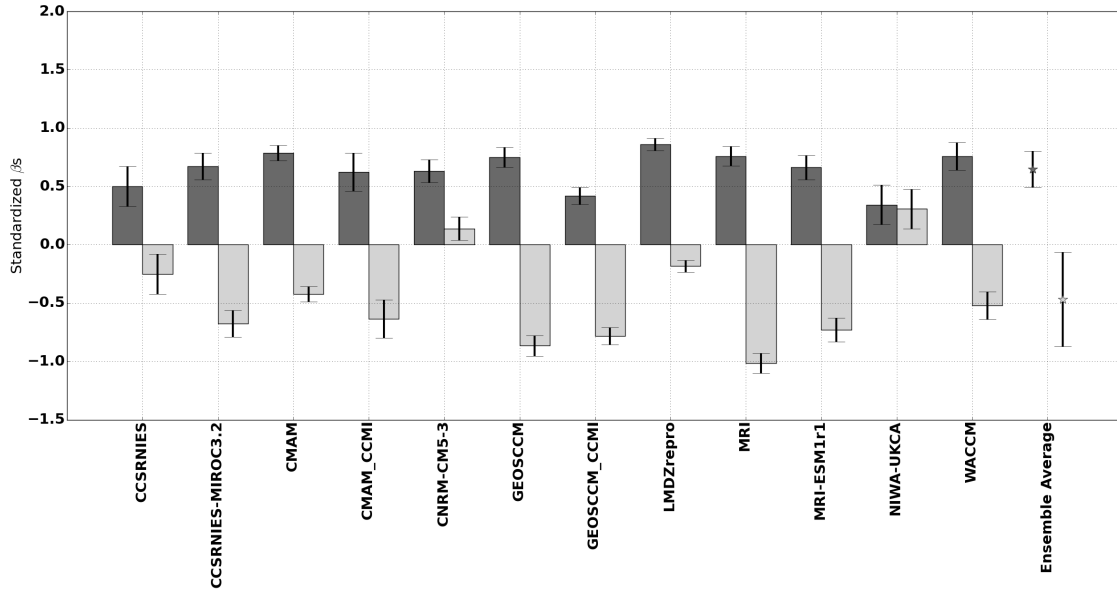
Figure 3.9: Each set of bars corresponds to the detrended regression coefficients ($\beta_{\Delta T}$ (dark grey) and β_{BDC} (light grey)) produced by MLR analysis after standardizing each variable (ΔT and BDC) by dividing out the time-series (2000-2097) $\pm$standard deviation, and error bars corresponding to each bar represents the uncertainty of each coefficient as the 95th percentile confidence interval. Detrended CCM ensemble average values for $\beta_{\Delta T}$ (dark grey) and β_{BDC} (light grey) are both represented by a $\star$, and corresponding error bars show variability (as the standard deviation) in all CCM $\pm$standardized regression coefficients.

Investigating the detrended MLRs, Figure 3.9 shows that both ΔT and BDC contributions to the interannual variability on $[H_2O]_{entry}$ are about equal, with the contribution of ΔT being slightly larger. Standardized ΔT regression coefficients from the detrended MLRs are similar in magnitude and average about 0.7 ± 0.1. We see that ΔT's contributes less to the interannual variability of $[H_2O]_{entry}$ than it does to long-term variability of

$[H_2O]_{entry}$. Average contribution of the BDC to interannual $[H_2O]_{entry}$ variability between all CCMs is about -0.4±0.3. Similar variability in individual BDC detrended standardized coefficient values exist as shown in Figure 3.8, however the BDC contributes more to the interannual variability of $[H_2O]_{entry}$ than to its long-term variability.

3.6   Century Regression Conclusion

We show that Century MLR analysis does a good job explaining the long-term trends and internanual variability in $[H_2O]_{entry}$ in the CCMs. Increases in ΔT produce increases in $[H_2O]_{entry}$. Increases in the strength of the BDC produce negative changes in $[H_2O]_{entry}$, which offset some, but not all, of the increase due to ΔT.

4. DECADAL REGRESSIONS

4.1 Why Decadal Regressions?

Ideally, we would compare the results of the previous chapter to observations. Unfortunately, we don't have 100 years of observations to test the models against. Instead, we will compare 10-year segments from the model to regressions of 10-years of observations Dessler et al. (2014).

4.2 Decadal Regression Equation

We use the same regression equation used in previous chapters to analyze $[H_2O]_{entry}$ monthly anomalies (defined in Appendix A.2) (Equation 4.1). Specifically, we split the reference-period into 10 time-frames (2000-2010,2010-2020,2020-2030,2040-2050,etc.) and examine each time-frame using a MLR (hereby decadal MLR). Monthly anomalies are calculated for each time-frame by subtracting the average annual cycle of each variable from monthly average values.

$$[H_2O]_{entry} = \beta_0 + \beta_{\Delta T}\Delta T_{lag3} + \beta_{BDC}\Delta BDC_{lag1} + \beta_{QBO}\Delta QBO_{lag3} + \epsilon \qquad (4.1)$$

β_0, β_1, and β_2 represent the same slope terms as represented in chapter 4, while β_3 is the slope term explaining how $[H_2O]_{entry}$ varies with the QBO in ppmv. Primary differences between the decadal and century MLR terms are: 1) For the decadal MLRs, each regression term discussed in this chapter refers to its monthly anomaly as opposed to annual anomalies discussed in chapter 4. 2) Decadal regression terms are lagged in order to maximize the amount of explained variance: we lag ΔT by 3 months, the BDC by 1 month, and the QBO by 3 months. We chose these lags to be the same as those used by *Dessler et al.* [2014]. Additionally, these lags are all plausible because it takes time for each regression

coefficient to impact $[H_2O]_{entry}$.

4.3 Decadal Explained Variance

Figure 4.1 shows the median±one standard deviation value of the decadal adjusted R^2 values generated by each CCM. The model average adjusted R^2 is approximately 0.6±0.25, indicating that there exists a large spread in the ability of the MLR to fit $[H_2O]_{entry}$ in the models. Several CCM decadal MLRs explain a large portion of $[H_2O]_{entry}$ variability (large decadal adjusted R^2 values). CCSRNIES-MIROC3.2, CMAM, CMAM-CCMI, GEOSCCM, GEOSCCM-CCMI, MRI, MRI-ESM1r1 all explain >60% of the variance in $[H_2O]_{entry}$. These R^2 are similar to the values obtained by MLR of observations performed by [*Dessler et al.*, 2014].

However, decadal MLR analysis does not work well with all CCMs. The CCSRNIES, CNRM-CM5-3, and NIWA-UKCA have decadal adjusted R^2 values approximately <0.4. Above this, but below the observations, is the LMDZrepro, which has a median decadal adjusted R^2 values of 0.5.
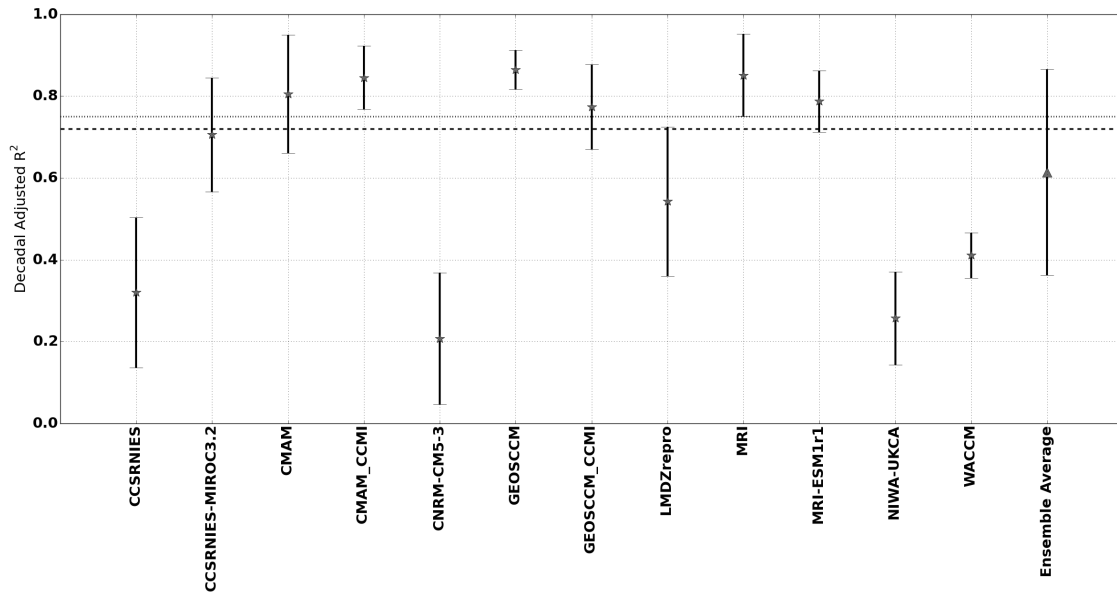
Figure 4.1: Each $\star$ represents the median decadal adjusted R^2 value for each CCM, and the error bars correspond to the $\pm$standard deviation of the range of each decadal adjusted R^2 distribution. The $\triangle$, corresponds to the CCM ensemble average decadal adjusted R^2 value, and the error bars correspond to the $\pm$standard deviation of the range of all (every CCM) decadal adjusted R^2 values. Found by *Dessler et al.* [2014], each line corresponds to observational-based MLR adjusted R^2 values (eraI (dotted) and MERRA (dashed)).

4.4 Physical Process Effects

Similar to the century MLRs, we can examine each physical process's contribution to $[H_2O]_{entry}$ monthly anomalies and compare those to observational MLR of *Dessler et al.* [2014]. For each model, we will calculate the median and standard deviation of each decadal regression coefficient for comparison. By examining which CCM decadal regression coefficients fall within 95% confidence of the observational-based coefficients, we can identify CCMs realistically capturing each physical process's effect on $[H_2O]_{entry}$, and determine which CCMs are doing the best job on shorter timescales.
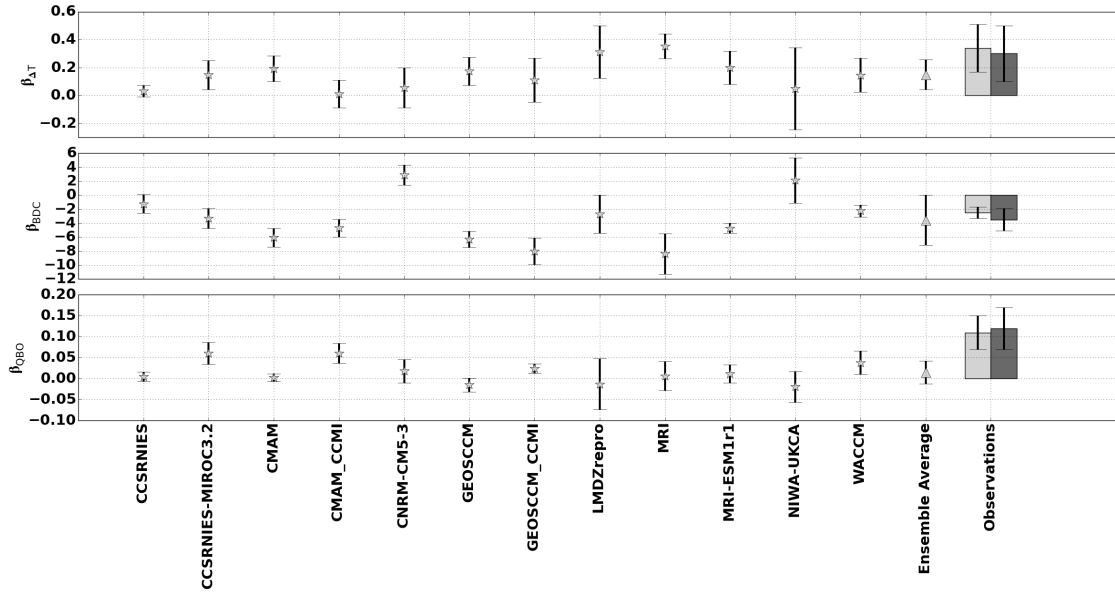
Figure 4.2: For each distribution of CCM decadal MLR regression coefficients ($\beta_{\Delta T}$, β_{BDC}, and β_{QBO}), Each $\star$ represents each median decadal regression coefficient, and associated error bars correspond to variability ($\pm$one standard deviation) of each distribution of regression coefficients. Each $\triangle$ represents the mean regression coefficient of the set of all coefficients from all CCMs, and associated error bars correspond to total variability ($\pm$one standard deviation) in all coefficients. Observational-based (eraI (light grey) and MERRA (dark grey)) coefficients obtained by *Dessler et al.* [2014] are represented by each bar, and associated error bars represent the uncertainty (95th percentile confidence interval) of each Observational-based regression coefficient.

4.4.1 Tropospheric Warming

On decadal timescales, Figure 4.2 shows the model ensemble average $[H_2O]_{entry}$ increases by about 0.18$\pm$0.2 ppmv K^{-1} and range between about 0 and 0.35 ppmv K^{-1}. Only the MRI ΔT regression coefficient distribution is large in comparison to all other CCMs at about 0.37$\pm$0.05. Most CCM decadal ΔT regression coefficient distributions are confined to a narrow range between approximately $\pm$0.1 ppmv K^{-1}. However, both the LMDZrepro and NIWA-UKCA ΔT regression coefficient distributions are large in comparison with a range of $\pm$0.4 ppmv K^{-1}.

In comparison to both observational-based ΔT regression coefficients, the MERRA ΔT regression coefficient is 0.30±0.20 ppmv K^{-1} and the eraI coefficient is 0.34±0.17 ppmv K^{-1}. Looking at the CCM consensus ΔT regression coefficient distribution, the CCM decadal MLRs generate ΔT regression coefficients smaller than both observational-based values. Thus, less CCM tropospheric water vapor is advected into the lower stratosphere as a result of interannual ΔT variability than in observations. Most CCM decadal ΔT regression coefficients fall within 95% confidence of both observational-based values. The only CCM decadal ΔT regression coefficient distribution not contained within MERRA ΔT 95% confidence are CCSRNIES and CMAM-CCMI, and the only decadal ΔT regression coefficient distributions not contained by eraI ΔT 95% confidence are CCSRNIES, CMAM-CCMI, and CNRM-CM5-3.

4.4.2 Brewer-Dobson Circulation

From Figure 4.2, we see that there exists a high degree of variability in the CCM decadal BDC regression coefficients, with a CCM ensemble average value of about -4±2 ppmv $(K/Day)^{-1}$. Investigating variability of individual CCM decadal BDC regression coefficients, all CCMs, except LMDZrepro, MRI, and NIWA-UKCA, decadal BDC regression coefficients range between approximately ±1 ppmv $(K/Day)^{-1}$. LMDZrepro, MRI, and NIWA-UKCA decadal BDC regression coefficients exist over a much wider range with values between approximately ±2 ppmv $(K/Day)^{-1}$. As we expect for longer timescales, a strengthening BDC should cool the TTL and reduce $[H_2O]_{entry}$ entering the lower stratosphere. CNRM-CM5-3 and NIWA-UKCA generate coefficients contrary to our expectations. Both models show that $[H_2O]_{entry}$ decreases by about 2 ppmv $(K/Day)^{-1}$ as a result of a strengthening BDC. All other CCMs produce negative decadal BDC regression coefficients.

From *Dessler et al.* [2014], using eraI reanalysis as a surrogate for the atmosphere, a

strengthening BDC reduces observed $[H_2O]_{entry}$ by -2.51±0.83 ppmv (K/Day)$^{-1}$, whereas MERRA reanalysis reduces observed $[H_2O]_{entry}$ entering the lower stratosphere by -3.48±1.62. Thus, eraI produces a higher degree of confidence in the BDC's effect on $[H_2O]_{entry}$ than MERRA. We expect more CCM decadal BDC regression coefficients to fall within 95% confidence of the MERRA regression coefficient than the eraI coefficient. In fact, CC-SRNIES, CCSRNIES-MIROC-3.2, CMAM, CMAM-CCMI, LMDZrepro, MRI-ESM1r1, and WACCM decadal BDC regression coefficients fall within 95% confidence of MERRA, and only CCSRNIES, LMDZrepro, and WACCM generate realistic decadal BDC regression coefficient in comparison to eraI. Even with individual CCM decadal BDC regression coefficients occurring over a larger range of values, the CCM ensemble average median decadal BDC regression coefficient is contained within 95% confidence of both observational-based coefficients. Observational regressions verify that, on decadal timescales, $[H_2O]_{entry}$ should decrease with a strengthening BDC. As discussed previously, CNRM-CM5-3 and NIWA-UKCA BDC regression coefficient distributions are both >0, indicating possible issues with these models simulation of the BDC's interaction with TTL temperatures.

4.4.3 Quasi-Biennial Osscilation

Figure 4.2 shows that the CCM ensemble average decadal QBO coefficient is approximately 0.03±0.04 ppmv. The largest increases in $[H_2O]_{entry}$ occur in CCSRNIES-MIROC3.2 and CMAM-CCMI with $[H_2O]_{entry}$ increasing by approximately 0.07 ppmv as the QBO strengthens. For all other CCMs, $[H_2O]_{entry}$ remains about constant as the QBO strengthens with decadal QBO regression coefficients either ranging about zero or within 0.02 ppmv of zero. Most CCM decadal QBO regression coefficient distributions are confined to a narrow range of values, $\leq |0.02|$ ppmv, however MRI and NIWA-UKCA decadal MLRs generate a large range of coefficients in comparison, approximately ±0.05.

It is clear that the QBO's impact on $[H_2O]_{entry}$ is underestimated by the CCMs investigated, with all decadal MLRS generating QBO regression coefficients smaller than the observational-based coefficients (MERRA coefficient: 0.09 ± 0.05 ppmv, eraI coefficient: 0.11 ± 0.04 ppmv). Only CCSRNIES-MIROC3.2 and CMAM-CCMI decadal MLRs produce at least a portion of QBO regression coefficients falling within 95% confidence of both observational-based coefficients. Two possible reasons exist to explain. First, simply, the CCM does not simulate a QBO [*SPARC*, 2010; *Morgenstern et al.*, 2010; *Eyring et al.*, 2013], or the QBO's impact on the lower stratosphere is poorly simulated. *Anstey et al.* [2016] found that climate models, generally, struggle to replicate the QBO's penetration into the lower stratosphere. As a result, they incorrectly impact TTL temperatures, and subsequently $[H_2O]_{entry}$.

4.5 Physical Process Relative Magnitude

When standardized, all three variables contribute approximately equally to $[H_2O]_{entry}$ variance on decadal timescales in the observations (Figure 4.3). In the CCMs, on the other hand, the BDC impacts $[H_2O]_{entry}$ more than ΔT, with standardized decadal ΔT regression coefficients on the order of about 0.3 and BDC regression coefficients on the order of about -0.4. For both models, CCSRNIES-MIROC3.2 and CMAM-CCMI, producing similar decadal QBO regression coefficients to the observational-based regressions, we see that the QBO also impacts $[H_2O]_{entry}$ more than ΔT, on the order of 0.5. Over longer timescales, we found that tropospheric water vapor advected into the lower stratosphere as a result of tropospheric warming acts to increase $[H_2O]_{entry}$ more than cooling the TTL with a strengthening BDC reduces $[H_2O]_{entry}$. On decadal timescales, long-term trends in ΔT are not evident, and as a result increases in tropospheric water vapor available for advection into the lower stratosphere do not have as large of an impact.

41
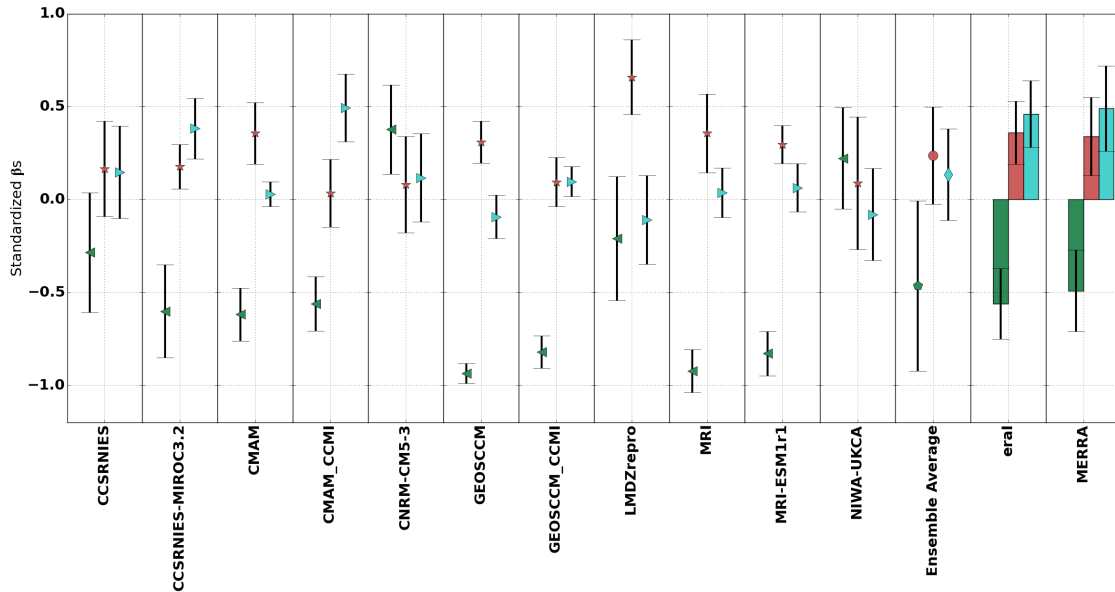
Figure 4.3: This plot displays the set of standardized decadal regression coefficients. Focusing on individual CCM distributions, $\beta_{\Delta T}$ (red ⋆), β_{BDC} (green ◁), and β_{QBO} (turquoise ▷) coefficients correspond to the median value of each coefficient distribution, and associated error bars correspond to variability (±one standard deviation) of each distribution. Focusing on a combined set of all CCM decadal regression coefficients, each coefficient, $\beta_{\Delta}T$ (red ⋆), β_{BDC} (green ◁), and β_{QBO} (turquoise ▷) represents the ensemble average, and associated error bars corresponds to variability (±one standard deviation) in the entire ensemble. Observational-based coefficients, found in *Dessler et al.* [2014], correspond to bars, $\beta_{\Delta T}$ (red), β_{BDC} (green), and β_{QBO} (turquoise), plotted with corresponding error bars representing the uncertainty (95th percentile confidence interval) of the observational-based coefficients

4.6 Century and Decadal Regression Coefficient Comparison

One question we yet directly addressed is, how do the regression coefficients corresponding to the simulated century and decadal MLRs compare? First, we compare each ΔT coefficient. From Figure 4.4, the trended ΔT coefficient is larger than the decadal ΔT coefficient for all CCMs. These simulations, following the A1B scenario [*IPCC*, 2001], warm the climate by approximately 3.5° C, and they also simulate increasing $[H_2O]_{entry}$. As mentioned prior, on century time-scales, we show ΔT is primarily responsible for 21st

42

century $[H_2O]_{entry}$ increases. Again, On short time-scales, long-term ΔT trends are not as evident. So, the century ΔT coefficients must be larger than the decadal ΔT coefficients to account for long-term increases in both ΔT and $[H_2O]_{entry}$. With respect to the BDC regression coefficients for both time-scales, Figure 4.4 shows most CCM (trended and decadal) BDC coefficients are similar in magnitude with most CCM century coefficients not deviating much from their decadal counterparts. By comparing the detrended regression coefficients to the decadal regression coefficients (not shown) and the standardized (trended and detrended) regression coefficients to the decadal regression coefficients, we find conclusions to end up being the same.
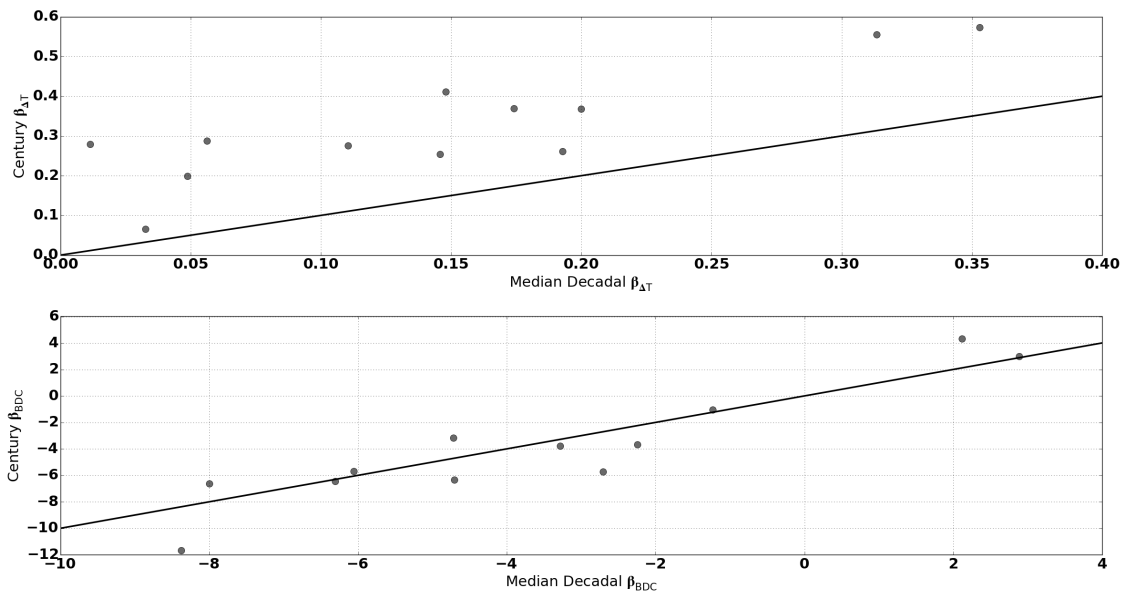
Figure 4.4: Scatter plots of (upper) trended ΔT regression coefficients (ppmv K^{-1}) vs. decadal ΔT regression coefficients (ppmv K^{-1}), and (lower) trended BDC regression coefficients (ppmv (K/Day)$^{-1}$) vs. decadal BDC regression coefficients (ppmv (K/Day)$^{-1}$). Black lines in both plots correspond to a 1:1 relationship.

43

4.7 Decadal Regression Conclusion

We find that not only can we use MLR analysis to predict monthly anomolies of $[H_2O]_{entry}$, but several CCM decadal MLRs actually explain more $[H_2O]_{entry}$ variance than the observational-based regressions. Analyzing how CCM decadal regression coefficients compare to observational-based coefficients, we find that: 1) all CCMs generate decadal ΔT regression coefficients contained within 95% confidence of both observational-based ΔT coefficients 2) There is more variance in decadal BDC regression coefficients than the other regression coefficients, and only CCSRNIES, CCSRNIES-MIROC3.2, LMDZre-pro, and WACCM BDC regression coefficients fall within 95% confidence of both observational-based BDC coefficients 3) Of the CCMs that simulate a QBO, only CCSRNIES-MIROC3.2 and CMAM-CCMI produce regression coefficients similar to observational-based coefficients. Additionally, both the BDC and QBO impact monthly anomalies of $[H_2O]_{entry}$ more than ΔT.

5. CONCLUSIONS

Can we model $[H_2O]_{entry}$ simulated during the 21st century using a MLR? To answer this question, we fit CCM $[H_2O]_{entry}$ by regressing three processes (ΔT, the BDC, and the QBO) important to $[H_2O]_{entry}$. Specifically, we analyze $[H_2O]_{entry}$ on two separate time-scales: 1) across the entire 21st century, and 2) on decadal timescales. For our analysis of the entire 21st century, we fit $[H_2O]_{entry}$ using ΔT and the BDC as explanatory variables. We do not include QBO variations in this analysis, because it has been shown that the QBO's effect on TTL temperatures is poorly simulated [*Anstey et al.*, 2016]. we produce MLRs of $[H_2O]_{entry}$ on decadal time-scales, because long-term datasets of observational $[H_2O]_{entry}$ are not available. [*Dessler et al.*, 2013, 2014] use the same methodology to analyze 2004-2014 MLS $[H_2O]_{entry}$. We compare MLR regression coefficients corresponding to those simulated $[H_2O]_{entry}$ to those found by *Dessler et al.* [2014]. Our analysis on decadal time-scales as opposed to century time-scales includes the QBO as one of the regression coefficients, because it significantly improves the fit of each decadal MLR.

5.1 Century Multivariate Linear Regressions

By investigating tropical annual $[H_2O]_{entry}$ simulated over the 21st century, all CCMs predict $[H_2O]_{entry}$ will increase as the climate warms, and century MLRs largely capture simulated long-term trends with adjusted R^2 values >0.85. Not only are we concerned with effectively reproducing $[H_2O]_{entry}$, but we want to capture its variability as well. Because long-term trends can artificially inflate adjusted R^2, we detrend each variable by filtering out variability of >10 years essentially focusing on interannual variance. After detrending the data, we re-run the MLR and analyze the results. By removing any influence long-term trends may have on the MLR, we see that most models not only replicate

$[H_2O]_{entry}$ long-term trends, but also accurately reproduce $[H_2O]_{entry}$ interannual variability with detrended adjusted R^2 values >0.7. However, this is not the case for all models. For instance, a detrended MLR of NIWA-UKCA $[H_2O]_{entry}$ produces an adjusted R^2 value of approximately 0.2 indicating a poor fit to actual $[H_2O]_{entry}$.

In analyzing the century MLR regression coefficients, we see that ΔT corresponds to more water vapor entering the lower stratosphere. A strengthening BDC, however, results in less water vapor transported into the lower stratosphere, because a strengthing BDC cools the TTL [*Butchart et al.*, 2006; *Li et al.*, 2007; *Garcia and Randel*, 2008; *Bönisch et al.*, 2011; *Castanheira et al.*, 2012; *Fu et al.*, 2015]. Also, on century time-scales, we find ΔT to be the most important of the two processes analyzed to $[H_2O]_{entry}$ increases simulated by CCMs.

5.2   Decadal Multivariate Linear Regressions

Looking at $[H_2O]_{entry}$ variability on decadal time-scales, we show that decadal MLRs, for most CCMs, explain much of the variability in $[H_2O]_{entry}$ with adjusted R^2 values typically >0.7. Additionally, several CCM decadal regressions actually outperform both observation-based regressions investigated in *Dessler et al.* [2014]. However, a large spread in adjusted R^2 values (about ± 0.2) does exist among CCMs with certain CCMs (CCSRNIES, CNRM-CM5-3 and NIWA-UKCA) decadal MLRs performing poorly based on adjusted R^2. Additionally, CCMs corresponding to small decadal MLR adjusted R^2 values are (except CNRM-CM5-3) the same CCMs corresponding to small detrended MLR adjusted R^2 values.

Investigating how CCM decadal regression coefficients compare to the observational-based coefficients, we see several key characteristics. First, simulated decadal ΔT regression coefficients are all contained within both observational-based ΔT 95% confidence. There is more variance among simulated decadal BDC coefficients, and only CCSRNIES,

CCSRNIES-MIROC3.2, LMDZrepro, and WACCM decadal MLRs generate BDC coefficients similar (within 95% confidence of) to the observational-based coefficients. Most CCMs do not simulate a QBO. So, for most CCMs, the QBO coefficient is approximately zero. Even among CCMs that do simulate a QBO, only CCSRNIES-MIROC3.2 and CMAM-CCMI coefficients are similar to both observation-based coefficients.

REFERENCES

Alcala, C. M., and A. E. Dessler (2002), Observations of deep convection in the trop-
ics using the tropical rainfall measuring mission (trmm) precipitation radar, *Jour-
nal of Geophysical Research: Atmospheres*, *107*(D24), AAC 17–1–AAC 17–7, doi:
10.1029/2002JD002457, 4792.

an Chen, C., J.-Y. Yu, and C. Chou (2016), Impacts of vertical structure of convection
in global warming: The role of shallow convection., *J. Climate*, *29*(12), 4665–4684,
doi:10.1175/JCLI-D-15-0563.1.

Anstey, J. A., J. F. Scinocca, and M. Keller (2016), Simulating the qbo in an atmospheric
general circulation model: Sensitivity to resolved and parameterized forcing, *J. Atmos.
Sci.*, *73*(4), 1649–1665, doi:10.1175/JAS-D-15-0099.1.

Arfeuille, F., et al. (2013), Modeling the stratospheric warming following the mt. pinatubo
eruption: uncertainties in aerosol extinctions, *Atmospheric Chemistry and Physics*,
13(22), 11,221–11,234, doi:10.5194/acp-13-11221-2013.

Austin, J., et al. (2003), Uncertainties and assessments of chemistry-climate models
of the stratosphere, *Atmospheric Chemistry and Physics*, *3*(1), 1–27, doi:10.5194/
acp-3-1-2003.

Austin, J., J. Wilson, and L. Feng (2007), Evolution of water vapor concentrations and
stratospheric age of air in coupled chemistry-climate model simulations., *J. Atmos. Sci.*,
64, 905–921, doi:10.1175/JAS3866.1.

Birner, T., and H. Bönisch (2011), Residual circulation trajectories and transit times into

the extratropical lowermost stratosphere, *Atmospheric Chemistry and Physics*, *11*(2), 817–827, doi:10.5194/acp-11-817-2011.

Bodeker, G. E., J. C. Scott, K. Kreher, and R. L. McKenzie (2001), Global ozone trends in potential vorticity coordinates using toms and gome intercompared against the dobson network: 1978-1998, *Journal of Geophysical Research: Atmospheres*, *106*(D19), 23,029–23,042, doi:10.1029/2001JD900220.

Bönisch, H., A. Engel, T. Birner, P. Hoor, D. W. Tarasick, and E. A. Ray (2011), On the structural changes in the brewer-dobson circulation after 2000, *Atmospheric Chemistry and Physics*, *11*(8), 3937–3948, doi:10.5194/acp-11-3937-2011.

Brewer, A. W. (1949), Evidence for a world circulation provided by the measurements of helium and water vapour distribution in the stratosphere, *Quarterly Journal of the Royal Meteorological Society*, *75*(326), 351–363, doi:10.1002/qj.49707532603.

Brunner, D., J. Staehelin, J. A. Maeder, I. Wohltmann, and G. E. Bodeker (2006), Variability and trends in total and vertically resolved stratospheric ozone based on the cato ozone data set, *Atmospheric Chemistry and Physics*, *6*(12), 4985–5008, doi: 10.5194/acp-6-4985-2006.

Butchart, N., et al. (2006), Simulations of anthropogenic change in the strength of the brewer-dobson circulation, *Clim. Dyn.*, *27*(7-8), 727–741, doi:10.1007/ s00382-006-0162-4.

Castanheira, J. M., T. R. Peevey, C. A. F. Marques, and M. A. Olsen (2012), Relationships between brewer-dobson circulation, double tropopauses, ozone and stratospheric water vapour, *Atmospheric Chemistry and Physics*, *12*(21), 10,195–10,208, doi: 10.5194/acp-12-10195-2012.

Chen, G., and L. Sun (2011), Mechanisms of the tropical upwelling branch of the brewer-dobson circulation: The role of extratropical waves., *J. Atmos. Sci.*, *68*(12), 2878–2892, doi:10.1175/JAS-D-11-044.1.

Choiu, E. W., L. W. Thomason, and W. P. Chu (2006), Variability of stratospheric water vapor inferred from sage ii, haloe, and boulder (colorado) balloon measurements., *J. Climate*, *19*, 4121–4133, doi:10.1175/JCLI3841.1.

Chou, C., and C.-A. Chen (2010), Depth of convection and the weakening of tropical circulation in global warming., *J. Climate*, *23*, 3019–3030, doi:10.1175/2010JCLI3383.1.

Corti, T., et al. (2008), Unprecedented evidence for deep convection hydrating the tropical stratosphere, *Geophysical Research Letters*, *35*(10), n/a–n/a, doi:10.1029/2008GL033641, 110810.

CPC (2016), QBO Index (NOAA Climate Prediction Center, College Park, MD), www.cpc.ncep.noaa.gov/data/indices, accessed: 2016-07-07.

Dessler, A., et al. (2016), Transport of ice into the stratosphere and the humidification of the stratosphere over the 21st century, *Geophysical Research Letters*, *43*(5), 2323–2329, doi:10.1002/2016GL067991, 2016GL067991.

Dessler, A. E. (1998), A reexamination of the "stratospheric fountain" hypothesis, *Geophysical Research Letters*, *25*(22), 4165–4168, doi:10.1029/1998GL900120.

Dessler, A. E. (2002), The effect of deep, tropical convection on the tropical tropopause layer, *Journal of Geophysical Research: Atmospheres*, *107*(D3), ACH 6–1–ACH 6–5, doi:10.1029/2001JD000511.

Dessler, A. E., M. R. Schoeberl, T. Wang, S. M. Davis, and K. H. Rosenlof (2013), Stratospheric water vapor feedback, *PNAS*, *110*(45), 18,087–18,091, doi:10.1073/pnas. 1310344110.

Dessler, A. E., M. R. Schoeberl, T. Wang, S. M. Davis, K. H. Rosenlof, and J.-P. Vernier (2014), Variations of stratospheric water vapor over the past three decades, *Journal of Geophysical Research: Atmospheres*, *119*(22), 12,588–12,598, doi:10.1002/ 2014JD021712, 2014JD021712.

Dhomse, S., M. Weber, I. Wohltmann, M. Rex, and J. P. Burrows (2006), On the possible causes of recent increases in northern hemispheric total ozone from a statistical analysis of satellite data from 1979 to 2003, *Atmospheric Chemistry and Physics*, *6*(5), 1165– 1180, doi:10.5194/acp-6-1165-2006.

Dobson, G. M. B. (1956), Origin and distribution of the polyatomic molecules in the atmosphere., *Proc. R. Soc. A*, *236*(1205), 187–193, doi:10.1098/rspa.1956.0127.

Donnelly, D. (2006), The fast fourier transform for experimentalist, part v: Filters., *Computing in Science and Engineering*, *8*(1), 92–95, doi:10.1109/MCSE.2006.14.

Dunkerton, T. (1978), On the mean meridional mass motions of the stratosphere and mesosphere., *J. Atmos. Sci.*, *58*(1), 7–25, doi:10.1175/1520-0469(1978)035⟨2325: OTMMMM⟩2.0.CO;2.

Evans, S. J., R. Toumi, J. E. Harries, M. R. Chipperfield, and J. M. Russell (1998), Trends in stratospheric humidity and the sensitivity of ozone to these trends, *Journal of Geophysical Research: Atmospheres*, *103*(D8), 8715–8725, doi:10.1029/98JD00265.

Eyring, V., et al. (2013), Overview of igac/sparc chemistry-climate model initiative (ccmi)

community simulations in support of upcoming ozone and climate assessments, *Tech. rep.*, Stratospheric Processes And their Role in Climate.

Flury, T., D. L. Wu, and W. G. Read (2013), Variability in the speed of the brewer-dobson circulation as observed by aura/mls, *Atmospheric Chemistry and Physics*, *13*(9), 4563–4575, doi:10.5194/acp-13-4563-2013.

Fu, Q., P. Lin, S. Solomon, and D. L. Hartmann (2015), Observational evidence of strengthening of the brewer-dobson circulation since 1980, *Journal of Geophysical Research: Atmospheres*, *120*(19), 10,214–10,228, doi:10.1002/2015JD023657, 2015JD023657.

Fueglistaler, S., and P. H. Haynes (2005), Control of interannual and longer-term variability of stratospheric water vapor, *Journal of Geophysical Research: Atmospheres*, *110*(D24), n/a–n/a, doi:10.1029/2005JD006019, d24108.

Fueglistaler, S., A. E. Dessler, T. J. Dunkerton, I. Folkins, Q. Fu, and P. W. Mote (2009a), Tropical tropopause layer, *Reviews of Geophysics*, *47*(1), n/a–n/a, doi:10.1029/2008RG000267, rG1004.

Fueglistaler, S., B. Legras, A. Beljaars, J.-J. Morcrette, A. Simmons, A. M. Tompkins, and S. Uppala (2009b), The diabatic heat budget of the upper troposphere and lower/mid stratosphere in ecmwf reanalyses, *Quarterly Journal of the Royal Meteorological Society*, *135*(638), 21–37, doi:10.1002/qj.361.

Fueglistaler, S., Y. S. Liu, T. J. Flannaghan, F. Ploeger, and P. H. Haynes (2014), Departure from clausius-clapeyron scaling of water entering the stratosphere in response to changes in tropical upwelling, *Journal of Geophysical Research: Atmospheres*, *119*(4), 1962–1972, doi:10.1002/2013JD020772.

Garcia, R. R., and W. J. Randel (2008), Acceleration of the brewer-dobson circulation due to increases in greenhouse gases, *J. Atmos. Sci.*, *65*, 2731–2739, doi:10.1175/2008JAS2712.1.

Garfinkel, C. I., D. W. Waugh, L. D. Oman, L. Wang, and M. M. Hurwitz (2013), Temperature trends in the tropical upper troposphere and lower stratosphere: Connections with sea surface temperatures and implications for water vapor and ozone, *Journal of Geophysical Research: Atmospheres*, *118*(17), 9658–9672, doi:10.1002/jgrd.50772.

Geller, M. A., and T. Zhou (2008), Morphology of tropical upwelling in the lower stratosphere, *J. Atmos. Sci.*, *65*, 2360–2374, doi:10.1175/2007JAS2421.1.

Geller, M. A., X. Zhou, and M. Zhang (2002), Simulations of the interannual variability of stratospheric water vapor, *J. Atmos. Sci.*, *59*, 1076–1085, doi:10.1175/1520-0469(2002)059⟨1076:SOTIVO⟩2.0.CO;2.

Gettelman, A., and Q. Fu (2002), A climatology of the tropical tropopause layer, *J. Meteor. Res. Japan*, *80*(4B), 911–924, doi:10.2151/jmsj.80.911.

Gettelman, A., W. J. Randel, F. Wu, and S. T. Massie (2002), Transport of water vapor in the tropical tropopause layer, *Geophysical Research Letters*, *29*(1), 9–1–9–4, doi:10.1029/2001GL013818.

Gettelman, A., P. M. d. F. Forster, M. Fujiwara, Q. Fu, H. Vmel, L. K. Gohar, C. Johanson, and M. Ammerman (2004), Radiation balance of the tropical tropopause layer, *J. Geophys. Res. Atmos.*, *109*(D7), n/a–n/a, doi:10.1029/2003JD004190, d07103.

Gettelman, A., et al. (2009), The tropical tropopause layer 1960-2100, *Atmospheric Chemistry and Physics*, *9*(5), 1621–1637, doi:10.5194/acp-9-1621-2009.

Gettelman, A., et al. (2010), Multimodel assessment of the upper troposphere and lower stratosphere: Tropics and global trends, *Journal of Geophysical Research: Atmospheres*, *115*(D3), n/a–n/a, doi:10.1029/2009JD013638, d00M08.

Gilford, D. M., S. Solomon, and R. W. Portmann (2016), Radiative impacts of the 2011 abrupt drops in water vapor and ozone in the tropical tropopause layer, *J. Climate*, *29*, 595–612, doi:10.1175/JCLI-D-15-0167.1.

Hanisco, T. F., et al. (2007), Observations of deep convective influence on stratospheric water vapor and its isotopic composition, *Geophysical Research Letters*, *34*(4), n/a–n/a, doi:10.1029/2006GL027899, l04814.

Hardiman, S. C., et al. (2015), Processes controlling tropical tropopause temperature and stratospheric water vapor in climate models., *J. Climate*, *28*, 6516–6535, doi:10.1175/JCLI-D-15-0075.1.

Haynes, P. H., C. J. Marks, M. E. McIntry, T. G. Shepherd, and K. P. Shine (1991), On the "Downward Control" of extratropical diabatic circulation by eddy-induced mean zonal forces, *J. Atmos. Sci.*, *48*(4), 651–678, doi:10.1175/1520-0469(1991)048⟨0651:OTCOED⟩2.0.CO;2.

Hegglin, M. I., et al. (2014), Vertical structure of stratospheric water vapour trends derived from merged satellite data, *Nat. Geosci.*, *7*(10), 768–776, doi:10.1038/ngeo2236.

Holton, J. R., and A. Gettelman (2001), Horizontal transport and the dehydration of the stratosphere, *Geophysical Research Letters*, *28*(14), 2799–2802, doi:10.1029/2001GL013148.

Holton, J. R., P. H. Haynes, M. E. McIntyre, A. R. Douglass, R. B. Rood, and L. Phis-

ter (1995), Stratosphere-troposphere exchange, *Rev. Geophys.*, *33*(4), 403–439, doi: 10.1029/95RG02097.

Hood, L. L., and J. P. McCormack (1992), components of interannual ozone change based on nimbus 7 toms data, *Geophysical Research Letters*, *19*(23), 2309–2312, doi:10.1029/ 92GL02638.

Hurst, D. F., S. J. Oltmans, H. Vmel, K. H. Rosenlof, S. M. Davis, E. A. Ray, E. G. Hall, and A. F. Jordan (2011), Stratospheric water vapor trends over boulder, colorado: Analysis of the 30 year boulder record, *Journal of Geophysical Research: Atmospheres*, *116*(D2), n/a–n/a, doi:10.1029/2010JD015065, d02306.

IPCC (2001), Climate change 2001: The scientific basis: Contribution of working group 1 to the third assessment report of the intergovernmental panel on climate change, *Tech. rep.*, Intergovernmental Panel on Climate Change (IPCC), New York.

Jaccard, J., C. K. Wan, and R. Turrisi (1990), The detection and interpretation of inter-action effects between continuous variables in multiple regression, *Multivariate Behavioral Research*, *25*(4), 467–478, doi:10.1207/s15327906mbr2504_4.

Jain, S., A. R. Jain, and T. K. Mandal (2013), Role of convection in hydration of tropical utls: implication of aura mls long-term observations., *Annales Geophysicae*, *31*(5), 967–981, doi:10.5194/angeo-31-967-2013.

Jiang, J. H., B. Wang, K. Goya, K. Hocke, S. D. Eckermann, J. Ma, D. L. Wu, and W. G. Read (2004), Geographical distribution and interseasonal variability of tropical deep convection: Uars mls observations and analyses, *Journal of Geophysical Research: Atmospheres*, *109*(D3), n/a–n/a, doi:10.1029/2003JD003756, d03111.

Johnson, D. G., K. W. Jucks, W. A. Traub, and K. V. Chance (2001), Isotopic composition of stratospheric water vapor: Implications for transport, *Journal of Geophysical Research: Atmospheres*, *106*(D11), 12,219–12,226, doi:10.1029/2000JD900764.

Jones, R. L., J. A. Pyle, J. E. Harries, A. M. Zavody, J. M. Russell, and J. C. Gille (1986), The water vapour budget of the stratosphere studied using lims and sams satellite data, *Quarterly Journal of the Royal Meteorological Society*, *112*(474), 1127–1143, doi:10. 1002/qj.49711247412.

Joshi, M. M., and G. S. Jones (2009), The climatic effects of the direct injection of water vapour into the stratosphere by large volcanic eruptions, *Atmos. Chem. Phys.*, *9*(16), 6109–6118, doi:10.5194/acp-9-6109-2009.

Kawatani, Y., J. N. Lee, and K. Hamilton (2014), Interannual variations of stratospheric water vapor in mls observations and climate model simulations., *J. Atmos. Sci.*, *71*(11), 4072–4085, doi:10.1175/JAS-D-14-0164.1.

Keith, D. W. (2000), Stratosphere-troposphere exchange: Inferences from the isotopic composition of water vapor, *Journal of Geophysical Research: Atmospheres*, *105*(D12), 15,167–15,173, doi:10.1029/2000JD900130.

Khaykin, S., et al. (2009), Hydration of the lower stratosphere by ice crystal geysers over land convective systems, *Atmospheric Chemistry and Physics*, *9*(6), 2275–2287, doi: 10.5194/acp-9-2275-2009.

Khosrawi, F., et al. (2013), Assessment of the interannual variability and influence of the qbo and upwelling on tracer distributions of n2o and o3 in the tropical lower stratosphere, *Atmos. Chem. Phys.*, *13*(7), 3619–3641, doi:10.5194/acp-13-3619-2013.

Kim, J., and S.-W. Son (2015), Formation and maintenance of the tropical cold-point

tropopause in a dry dynamic-core gcm., *J. Atmos. Sci.*, *72*(8), 3097–3115, doi:10.1175/ JAS-D-14-0338.1.

Kirk-Davidoff, D. B., E. J. Hintsa, J. G. Anderson, and D. W. Keith (1999), The effect of climate change on ozone depletion through changes in stratospheric water vapour, *Nature*, *402*, 399–401, doi:10.1038/46521.

Kley, D., E. Stone, W. Henderson, J. Drummond, W. Harrop, A. Schmeltekopf, T. Thompson, and R. Winkler (1979), In situ measurements of the mixing ratio of water vapor in the stratosphere., *J. Atmos. Sci.*, *36*(12), 2513–2524, doi:10.1175/1520-0469(1979) 036⟨2513:smotmr⟩2.0.co;2.

Kuang, Z., G. C. Toon, P. O. Wennberg, and Y. L. Yung (2003), Measured hdo/h2o ratios across the tropical tropopause, *Geophysical Research Letters*, *30*(7), n/a–n/a, doi:10. 1029/2003GL017023, 1372.

Kulyamin, D. V., and V. P. Dymnikov (2014), The atmospheric general circulation model with a hybrid vertical coordinate, *Russian Journal of Numerical Analysis and Mathematical Modeling*, *29*(6), 355–373, doi:10.1515/rnam-2014-0029.

Li, F., J. Austin, and J. Wilson (2007), The strength of the brewer-dobson circulation in a changing climate: Coupled chemistry-climate model simulations, *J. Climate*, *21*, 40–57, doi:10.1175/2007JCLI1663.1.

Liang, C. K., A. Eldering, A. Gettelman, B. Tian, S. Wong, E. J. Fetzer, and K. N. Liou (2011), Record of tropical interannual variability of temperature and water vapor from a combined airs-mls data set, *J. Geophys. Res. Atmos.*, *116*(D6), n/a–n/a, doi:10.1029/ 2010JD014841, d06103.

Löffler, M., S. Brinkop, and P. Jöckel (2016), Impact of major volcanic eruptions on

stratospheric water vapour, *Atmospheric Chemistry and Physics*, *16*(10), 6547–6562, doi:10.5194/acp-16-6547-2016.

Manabe, S., and R. T. Wetherald (1967), Thermal equilibrium of the atmosphere with a given distribution of relative humidity, *J. Atmos. Sci.*, *24*(3), 241–259, doi:10.1175/ 1520-0469(1967)024⟨0241:TEOTAW⟩2.0.CO;2.

Marrow-Howell, N. (1994), The m word: Multicollinearity in multiple regression, *Social Work Research*, *18*(4), 247–251.

Mastenbrook, H. J. (1968), Water vapor distribution in the stratosphere and high tropo-sphere, *J. Atmos. Sci.*, *25*, 299–311, doi:10.1175/1520-0469(1968)025⟨0299:WVDITS⟩ 2.0.CO;2.

Mastenbrook, H. J. (1971), The variability of water vapor in the stratosphere, *J. Atmos. Sci.*, *28*, 1495–1501, doi:10.1175/1520-0469(1971)028⟨1495:TVOWVI⟩2.0.CO;2.

Maycock, A. C., J. M. Joshi, K. P. Shine, and A. A. Scaife (2013), The circulation response to idealized changes in stratospheric water vapor, *J. Climate*, *140*, 545–561, doi:10. 1002/qj.2287.

Maycock, A. C., M. M. Joshi, K. P. Shine, S. M. Davis, and K. H. Rosenlof (2014), The potential impact of changes in lower stratospheric water vapour on stratospheric temperatures over the past 30 years, *Quarterly Journal of the Royal Meteorological Society*, *140*(684), 2176–2185, doi:10.1002/qj.2287.

Montgomery, D. C., and E. A. Peck (1992a), *Multicollinearity*, chap. 8, John Wiley and Sons, Inc., New York.

Montgomery, D. C., and E. A. Peck (1992b), *Multiple Linear Regression*, chap. 4, John Wiley and Sons, Inc., New York.

Morgenstern, O., et al. (2010), Review of the formulation of present-generation stratospheric chemistry-climate models and associated external forcings, *Journal of Geophysical Research: Atmospheres*, *115*(D3), n/a–n/a, doi:10.1029/2009JD013728, d00M02.

Mote, P. W., K. H. Rosenlof, J. R. Holton, R. S. Harwood, and J. W. Waters (1995), Seasonal variations of water vapor in the tropical lower stratosphere, *Geophysical Research Letters*, *22*(9), 1093–1096, doi:10.1029/95GL01234.

Mote, P. W., et al. (1996), An atmospheric tape recorder: The imprint of tropical tropopause temperatures on stratospheric water vapor, *Journal of Geophysical Research: Atmospheres*, *101*(D2), 3989–4006, doi:10.1029/95JD03422.

Moyer, E. J., F. W. Irion, Y. L. Yung, and M. R. Gunson (1996), Atmos stratospheric deuterated water and implications for troposphere-stratosphere transport, *Geophysical Research Letters*, *23*(17), 2385–2388, doi:10.1029/96GL01489.

Newell, R. E., and S. Gould-Stewart (1981), A stratospheric fountain?, *J. Atmos. Sci.*, *38*(12), 2789–2796, doi:10.1175/1520-0469(1981)038⟨2789:ASF⟩2.0.CO;2.

Oltmans, S. J., H. Vmel, D. J. Hofmann, K. H. Rosenlof, and D. Kley (2000), The increase in stratospheric water vapor from balloonborne, frostpoint hygrometer measurements at washington, d.c., and boulder, colorado, *Geophys. Res. Lett.*, *27*(21), 3453–3456, doi:10.1029/2000GL012133.

Oman, L., D. W. Waugh, S. Pawson, R. S. Stolarski, and E. J. Nielsen (2008), Understanding the changes of stratospheric water vapor in coupled chemistry-climate model simulations., *J. Atmos. Sci.*, *65*, 3278–3291, doi:10.1175/2008JAS2696.1.

O'Sullivan, D., and T. J. Dunkerton (1997), The influence of the quasi-biennial oscillation

on global constituent distributions, *J. Geophys. Res. Atmos.*, *102*(D18), 21,731–21,743, doi:10.1029/97JD01689.

Paulik, L. C., and T. Birner (2012), Quantifying the deep convective temperature signal within the tropical tropopause layer (ttl), *Atmospheric Chemistry and Physics*, *12*(24), 12,183–12,195, doi:10.5194/acp-12-12183-2012.

Pearce, D. K., and S. A. Reiter (1985), Regression strategies when multicollinearity is a problem: A methodological note, *Journal of Accounting Research*, *23*(1), 405–407, doi:10.2307/2490928.

Peters, G. P., R. M. Andrew, T. Boden, J. G. Canadell, P. Ciais, C. L. Quere, G. Marland, M. R. Raupach, and C. Wilson (2013), The challenge to keep global warming below $2°$, *Nature Climate Change*, *3*, 4–6, doi:10.1038/nclimate1783.

Ploeger, F., M. Abalos, T. Birner, P. Konopka, B. Legras, R. Mller, and M. Riese (2015), Quantifying the effects of mixing and residual circulation on trends of stratospheric mean age of air, *Geophysical Research Letters*, *42*(6), 2047–2054, doi:10.1002/2014GL062927, 2014GL062927.

Posselt, D. J., S. van den Heever, G. Stephens, and M. R. Igel (2012), Changes in the interaction between tropical convection, radiation, and the large-scale circulation in a warming environment., *J. Climate*, *25*(2), 557–571, doi:10.1175/2011JCLI4167.1.

Poulain, V., et al. (2016), Evaluation of the inter-annual variability of stratospheric chemical composition in chemistry-climate models using ground-based multi-species time series, *J. Atmos. Sol.-Terr. Phys.*, *102*(4), 61–84, doi:10.1016/j.jastp.2016.03.010.

Randel, W. J., and F. Wu (2007), A stratospheric ozone profile data set for 1979-2005:

Variability, trends, and comparisons with column ozone data, *Journal of Geophysical Research: Atmospheres*, *112*(D6), n/a–n/a, doi:10.1029/2006JD007339, d06313.

Randel, W. J., F. Wu, J. M. Russell, A. Roche, and J. W. Waters (1998), Seasonal cycles and qbo variations in stratospheric ch4 and h2o observed in uars haloe data, *J. Atmos. Sci.*, *55*(2), 163–185, doi:10.1175/1520-0469(1998)055⟨0163:SCAQVI⟩2.0.CO;2.

Randel, W. J., F. Wu, H. Vmel, G. E. Nedoluha, and P. Forster (2006), Decreases in stratospheric water vapor after 2001: Links to changes in the tropical tropopause and the brewer-dobson circulation, *J. Geophys. Res. Atmos.*, *111*(D12), n/a–n/a, doi: 10.1029/2005JD006744.

Read, W. G., M. J. Schwartz, A. Lambert, H. Su, N. J. Livesey, W. H. Daffer, and C. D. Boone (2008), The roles of convection, extratropical mixing, and in-situ freeze-drying in the tropical tropopause layer, *Atmospheric Chemistry and Physics*, *8*(20), 6051–6067, doi:10.5194/acp-8-6051-2008.

Reed, R. J., W. J. Campbell, L. A. Rasmussen, and D. G. Rogers (1961), Evidence of a downward-propagating, annual wind reversal in the equatorial stratosphere, *Journal of Geophysical Research*, *66*(3), 813–818, doi:10.1029/JZ066i003p00813.

Reinsel, G. C., E. Weatherhead, G. C. Tiao, A. J. Miller, R. M. Nagatani, D. J. Wuebbles, and L. E. Flynn (2002), On detection of turnaround and recovery in trend for ozone, *Journal of Geophysical Research: Atmospheres*, *107*(D10), ACH 1–1–ACH 1–12, doi: 10.1029/2001JD000500.

Riviere, E. D., V. Marecal, N. Larsen, and S. Cautenet (2006), Modelling study of the impact of deep convection on the utls air composition – part 2: Ozone budget in the ttl., *Atmos. Chem. Phys.*, *6*(6), 1585–1598, doi:10.5194/acp-6-1585-2006.

Roscoe, H. K., and K. H. Rosenlof (2011), Revisiting the lower stratospheric water vapour trend from the 1950s to 1970s, *Atmospheric Science Letters*, *12*, 321–324, doi:10.1002/asl.339.

Rosenlof, K. H. (2003), How water enters the stratosphere., *Science*, *302*(5651), 1691–1692, doi:10.1126/science.1092703.

Rosenlof, K. H., and G. C. Reid (2008), Trends in the temperature and water vapor content of the tropical lower stratosphere: Sea surface connection, *Journal of Geophysical Research: Atmospheres*, *113*(D6), n/a–n/a, doi:10.1029/2007JD009109, d06107.

Rossow, W. B., and C. Pearl (2007), 22-year survey of tropical convection penetrating into the lower stratosphere, *Geophysical Research Letters*, *34*(4), n/a–n/a, doi:10.1029/2006GL028635, l04803.

Russo, M. R., et al. (2011), Representation of tropical deep convection in atmospheric models - part 1: Meteorology and comparison with satellite observations, *Atmos. Chem. Phys.*, *11*(6), 2765–2786, doi:10.5194/acp-11-2765-2011.

Sahany, S., J. D. Neelin, K. Hales, and R. B. Neale (2014), Deep convective transition characteristics in the community climate system model and changes under global warming., *J. Climate*, *27*(24), 9214–9232, doi:10.1175/JCLI-D-13-00747.1.

Santer, B. D., T. M. L. Wigley, J. S. Boyle, D. J. Gaffen, J. J. Hnilo, D. Nychka, D. E. Parker, and K. E. Taylor (2000), Statistical significance of trends and trend differences in layer-average atmospheric temperature time series, *Journal of Geophysical Research: Atmospheres*, *105*(D6), 7337–7356, doi:10.1029/1999JD901105.

Schieferdecker, T., S. Lossow, G. P. Stiller, and T. von Clarmann (2015), Is there a so-

lar signal in lower stratospheric water vapour?, *Atmospheric Chemistry and Physics*, *15*(17), 9851–9863, doi:10.5194/acp-15-9851-2015.

Sherwood, S. C. (2000), A stratospheric "drain" over the maritime continent, *Geophysical Research Letters*, *27*(5), 677–680, doi:10.1029/1999GL010868.

Sherwood, S. C., and A. E. Dessler (2000), On the control of stratospheric humidity, *Geophysical Research Letters*, *27*(16), 2513–2516, doi:10.1029/2000GL011438.

Sherwood, S. C., and A. E. Dessler (2001), A model for transport across the tropical tropopause, *J. Atmos. Sci.*, *58*, 765–779, doi:10.1175/1520-0469(2001)058⟨0765:AMFTAT⟩2.0.CO;2.

Sherwood, S. C., and A. E. Dessler (2003), Convective mixing near the tropical tropopause: Insights from seasonal variations., *J. Atmos. Sci.*, *60*(21), 2674–2685, doi:10.1175/1520-0469(2003)060⟨2674:cmnttt⟩2.0.co;2.

Sherwood, S. C., T. Horinouchi, and H. A. Zeleznik (2003), Convective impact on temperatures observed near the tropical tropopause, *J. Atmos. Sci.*, *60*, 1847–1855, doi:10.1175/1520-0469(2003)060⟨1847:CIOTON⟩2.0.CO;2.

Shindell, D. T. (2001), Climate and ozone response to increased stratospheric water vapor, *Geophysical Research Letters*, *28*(8), 1551–1554, doi:10.1029/1999GL011197.

Solomon, S., K. H. Rosenlof, R. W. Portmann, J. S. Daniel, S. M. Davis, T. J. Sanford, and P. Gian-Kasper (2010), Contributions of stratospheric water vapor to decadal changes in the rate of global warming, *Science*, *327*(5970), 1219–1223, doi:10.1126/science.1182488.

SPARC (2010), SPARC CCMVal Report on the Evaluation of Chemistry-Climate Models, *Tech. rep.*, Stratosphere-troposphere Processes and their role in climate (SPARC).

Stenke, A., and V. Grewe (2005), Simulation of stratospheric water vapor trends: impact on stratospheric ozone chemistry, *Atmospheric Chemistry and Physics*, *5*(5), 1257–1272, doi:10.5194/acp-5-1257-2005.

Stuber, N., M. Ponater, and R. Sausen (2001), Is the climate sensitivity to ozone perturbations enhanced by stratospheric water vapor feedback?, *Geophysical Research Letters*, *28*(15), 2887–2890, doi:10.1029/2001GL013000.

Svendby, T. M., and A. Dahlback (2004), Statistical analysis of total ozone measurements in oslo, norway, 1978-1998, *Journal of Geophysical Research: Atmospheres*, *109*(D16), n/a–n/a, doi:10.1029/2004JD004679, d16107.

Tan, J., C. Jakob, W. B. Rossow, and G. Tslioudis (2015), Increases in tropical rainfall driven by changes in frequency of organized deep convection., *Nature*, *519*(7544), 451–460, doi:10.1038/nature14339.

Tandon, N. F., L. M. Polvani, and S. M. Davis (2011), The response of troposheric circulation to water vapor-like forcings in the stratosphere, *J. Climate*, *24*(21), 5713–5720, doi:10.1175/JCLI-D-11-00069.1.

Tao, M., P. Konopka, F. Ploeger, J.-U. Grooß, R. Müller, C. M. Volk, K. A. Walker, and M. Riese (2015), Impact of the 2009 major sudden stratospheric warming on the composition of the stratosphere, *Atmos. Chem. Phys.*, *15*(15), 8695–8715, doi:10.5194/acp-15-8695-2015.

Ueyama, R., and J. M. Wallace (2010), To what extent does high-latitude wave forcing drive tropical upwelling in the brewer-dobson circulation?, *J. Atmos. Sci.*, *67*, 1242–1246, doi:10.1175/2009JAS3216.1.

Ueyama, R., E. J. Jensen, L. Pfister, and J.-E. Kim (2015), Dynamical, convective, and microphysical control on wintertime distributions of water vapor and clouds in the tropical tropopause layer, *Journal of Geophysical Research: Atmospheres*, *120*(19), 10,483–10,500, doi:10.1002/2015JD023318, 2015JD023318.

WMO (1998), Scientific assessment of ozone depletion: 1997, *Tech. Rep. 44*, Global Ozone Research and Monitoring Project, Geneva, Switzerland.

WMO (2007), Scientific assessment of ozone depletion: 2006, *Tech. Rep. 50*, Global Ozone Research and Monitoring Project, Geneva, Switzerland.

WMO (2011), Scientific assessment of ozone depletion: 2010, *Tech. Rep. 52*, Global Ozone Research and Monitoring Project, Geneva, Switzerland.

Wohltmann, I., R. Lehmann, M. Rex, D. Brunner, and J. A. Mder (2007), A process-oriented regression model for column ozone, *Journal of Geophysical Research: Atmospheres*, *112*(D12), n/a–n/a, doi:10.1029/2006JD007573, d12304.

Wohltmann, I., R. Lehmann, M. Rex, D. Brunner, and J. A. Mader (2008), Ozone trends at northern mid-and high latitudes-a european perspective, *Geophys: Atmos. Hydrospheres Space Sci.*, *26*(5), 1207–1220, doi:10.5194/angeo-26-1207-2008.

Wu, D. L., W. G. Read, A. E. Dessler, S. C. Sherwood, and J. H. Jiang (2005), Uars/mls cloud ice measurements: Implications for h2o transport near the tropopause, *J. Atmos. Sci.*, *62*(2), 518–530, doi:10.1175/JAS-3382.1.

Zhou, X. L., M. A. Geller, and M. H. Zhang (2001), Tropical cold point tropopause characteristics derived from ecmwf reanalyses and soundings, *J. Climate*, *14*, 1823–1838, doi:10.1175/1520-0442(2001)014⟨1823:TCPTCD⟩2.0.CO;2.

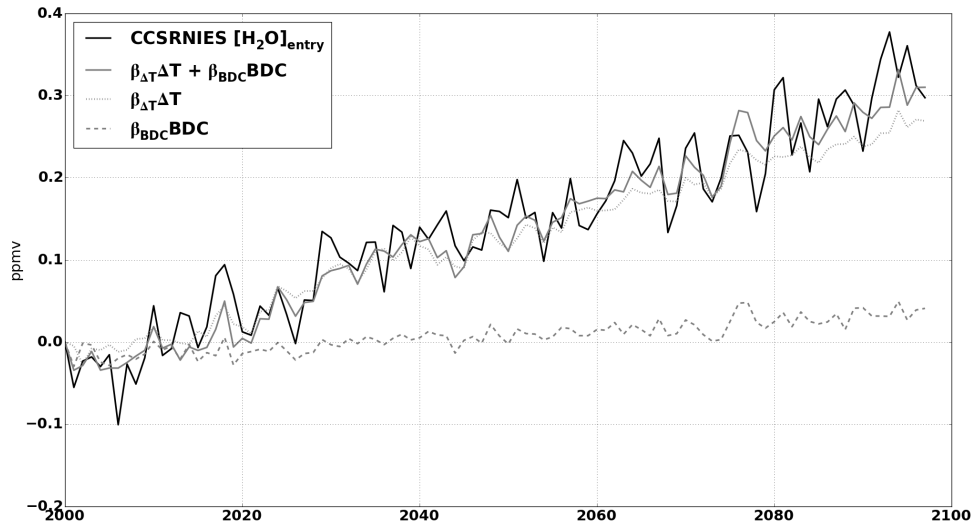OTHER CCM TRENDED MULTIVARIATE LINEAR REGRESSIONS

Figure A.1: 21st century annual anomalies of detrended $[H_2O]_{entry}$ from the CCSRNIES (black), and it reconstructed by a multivariate linear regression (gray) using ΔT and BDC (both not shown) annual anomalies as predictors. For this plot, all variables have been detrended by filtering long-term >10 years variations out.
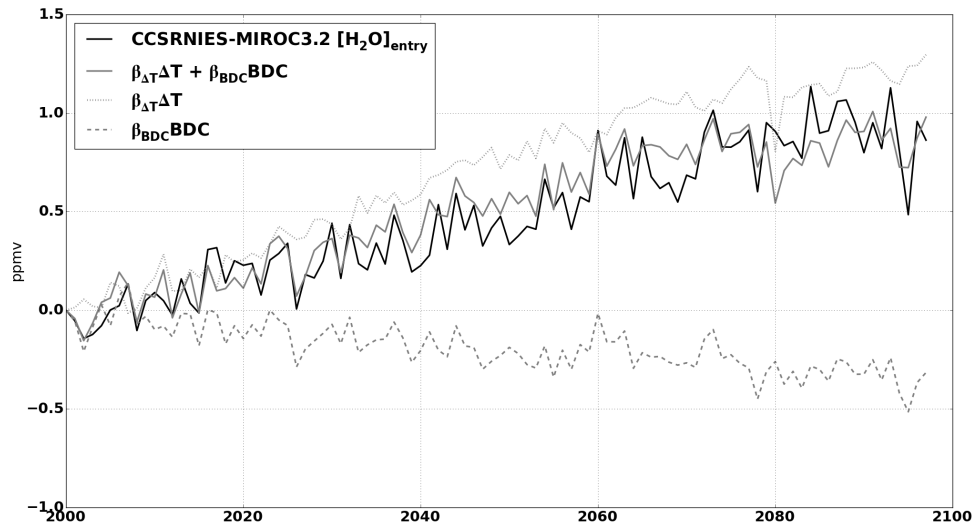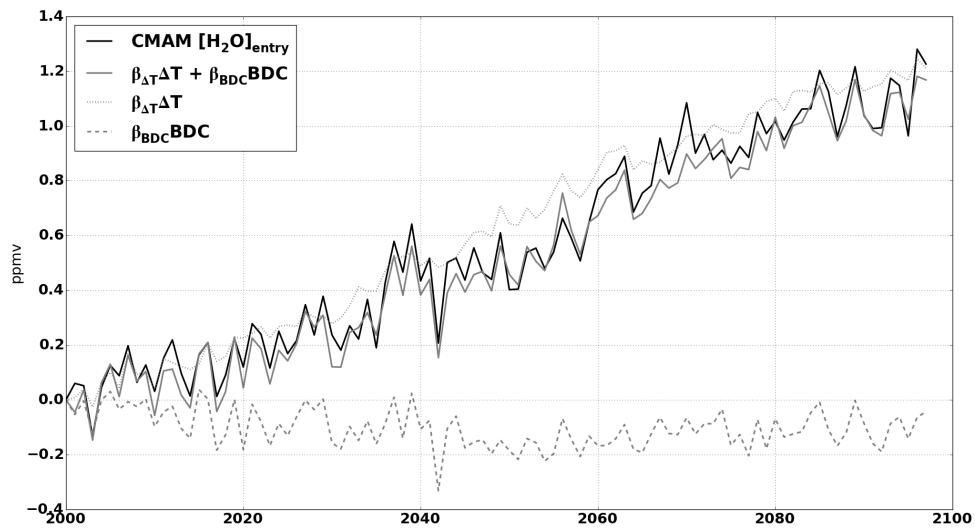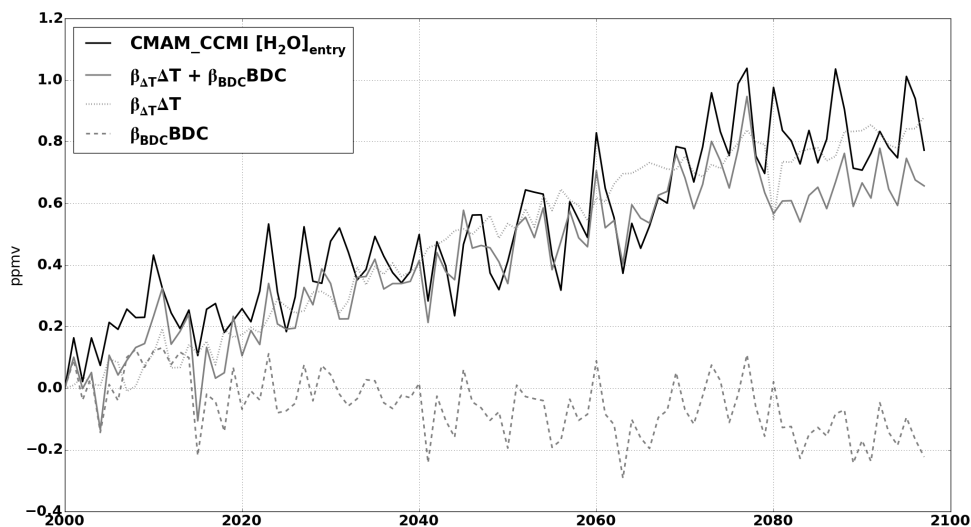
Figure A.2: 21st century annual anomalies of detrended $[H_2O]_{entry}$ from the CCSRNIES-MIROC3.2 (black), and it reconstructed by a multivariate linear regression (gray) using ΔT and BDC (both not shown) annual anomalies as predictors. For this plot, all variables have been detrended by filtering long-term >10 years variations out.

Figure A.3: 21st century annual anomalies of detrended $[H_2O]_{entry}$ from the CMAM (black), and it reconstructed by a multivariate linear regression (gray) using ΔT and BDC (both not shown) annual anomalies as predictors. For this plot, all variables have been detrended by filtering long-term >10 years variations out.
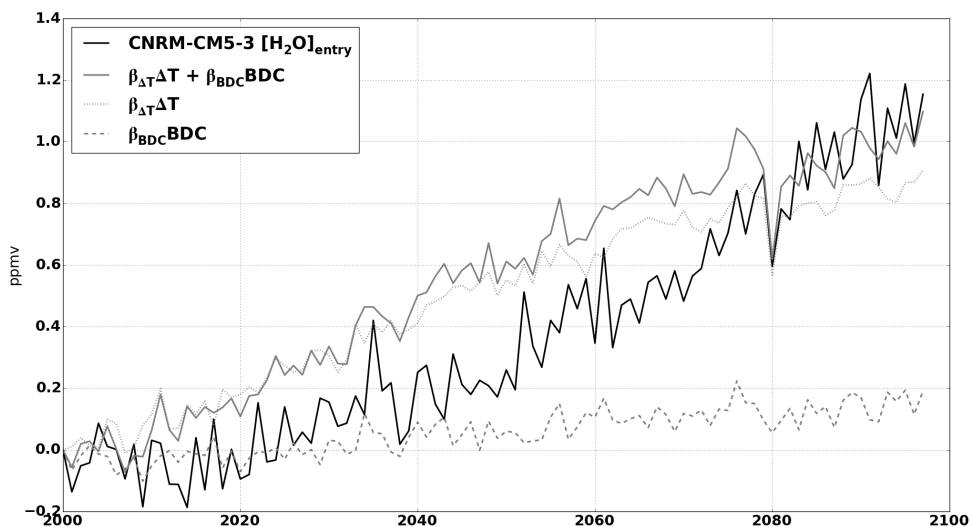
Figure A.4: 21st century annual anomalies of detrended $[H_2O]_{entry}$ from the CMAM-CCMI (black), and it reconstructed by a multivariate linear regression (gray) using ΔT and BDC (both not shown) annual anomalies as predictors. For this plot, all variables have been detrended by filtering long-term >10 years variations out.
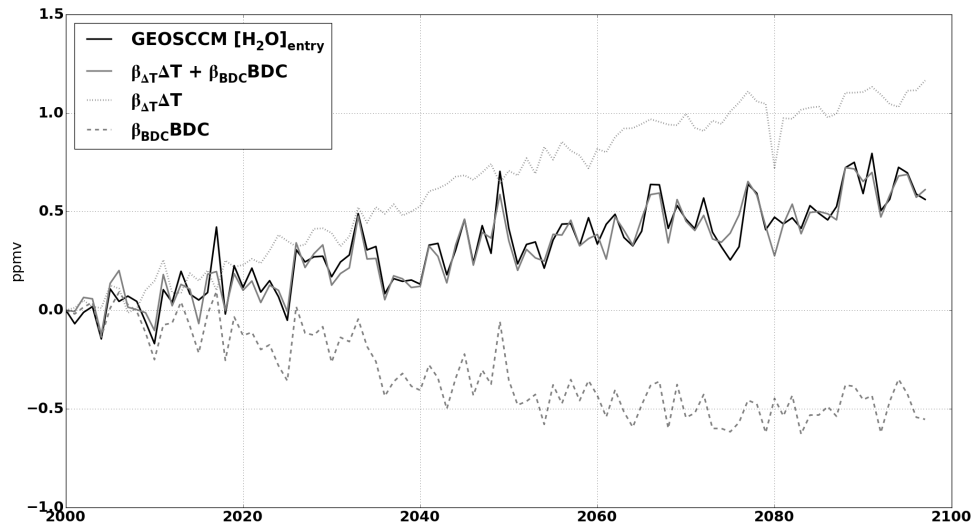

Figure A.5: 21st century annual anomalies of detrended $[H_2O]_{entry}$ from the CNRM-CM5-3 (black), and it reconstructed by a multivariate linear regression (gray) using ΔT and BDC (both not shown) annual anomalies as predictors. For this plot, all variables have been detrended by filtering long-term >10 years variations out.
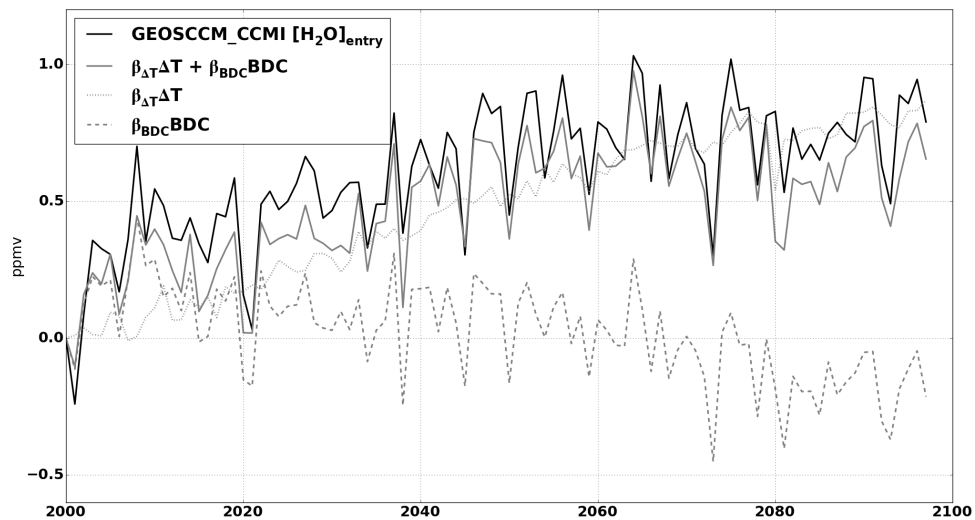
Figure A.6: 21st century annual anomalies of detrended $[H_2O]_{entry}$ from the GEOSCCM (black), and it reconstructed by a multivariate linear regression (gray) using ΔT and BDC (both not shown) annual anomalies as predictors. For this plot, all variables have been detrended by filtering long-term >10 years variations out.

Figure A.7: 21st century annual anomalies of detrended $[H_2O]_{entry}$ from the GEOSCCM-CCMI (black), and it reconstructed by a multivariate linear regression (gray) using ΔT and BDC (both not shown) annual anomalies as predictors. For this plot, all variables have been detrended by filtering long-term >10 years variations out.
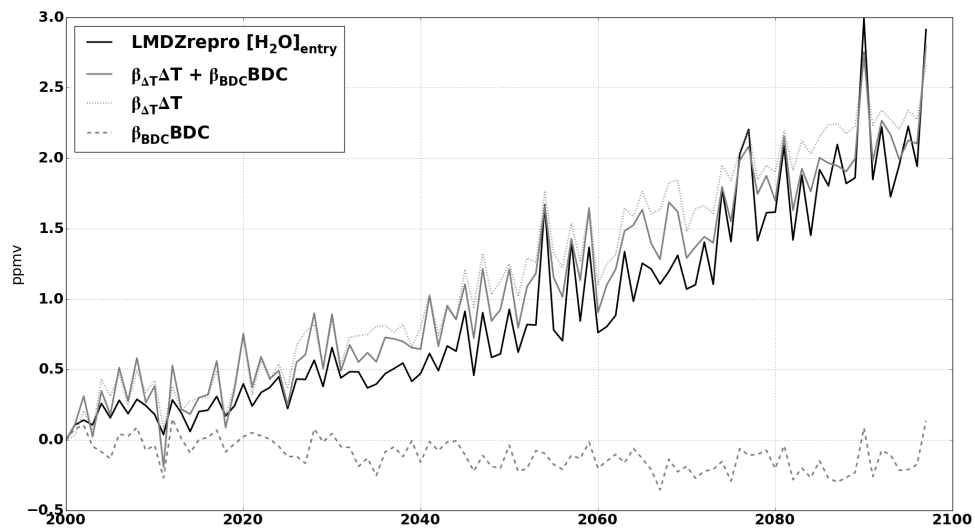
Figure A.8: 21st century annual anomalies of detrended $[H_2O]_{entry}$ from the LMDZrepro (black), and it reconstructed by a multivariate linear regression (gray) using ΔT and BDC (both not shown) annual anomalies as predictors. For this plot, all variables have been detrended by filtering long-term >10 years variations out.
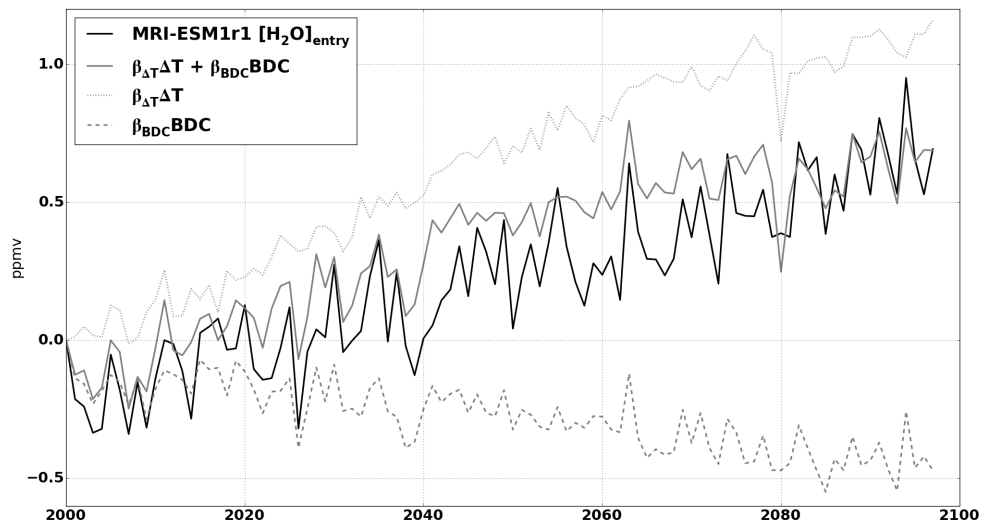
Figure A.9: 21st century annual anomalies of detrended $[H_2O]_{entry}$ from the MRI-ESM1r1 (black), and it reconstructed by a multivariate linear regression (gray) using ΔT and BDC (both not shown) annual anomalies as predictors. For this plot, all variables have been detrended by filtering long-term >10 years variations out.
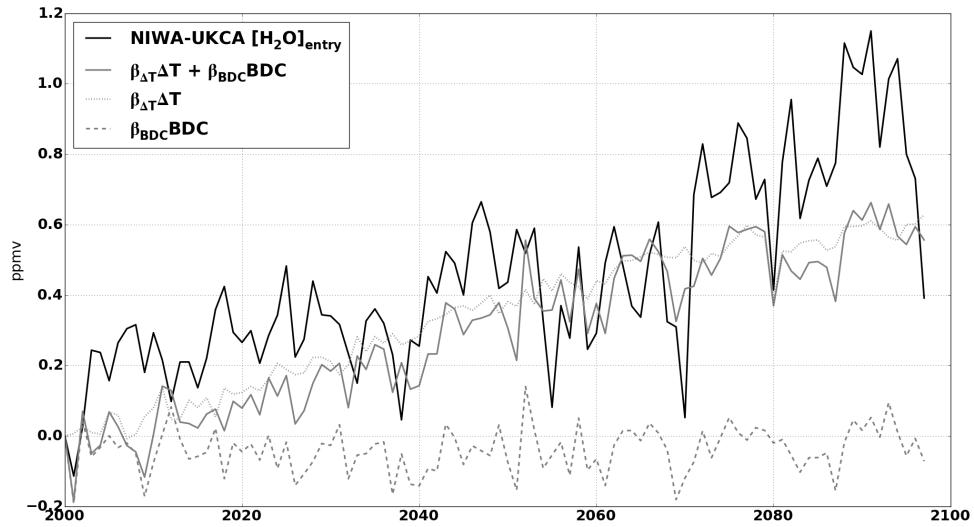
Figure A.10: 21st century annual anomalies of detrended $[H_2O]_{entry}$ from the NIWA-UKCA (black), and it reconstructed by a multivariate linear regression (gray) using ΔT and BDC (both not shown) annual anomalies as predictors. For this plot, all variables have been detrended by filtering long-term >10 years variations out.
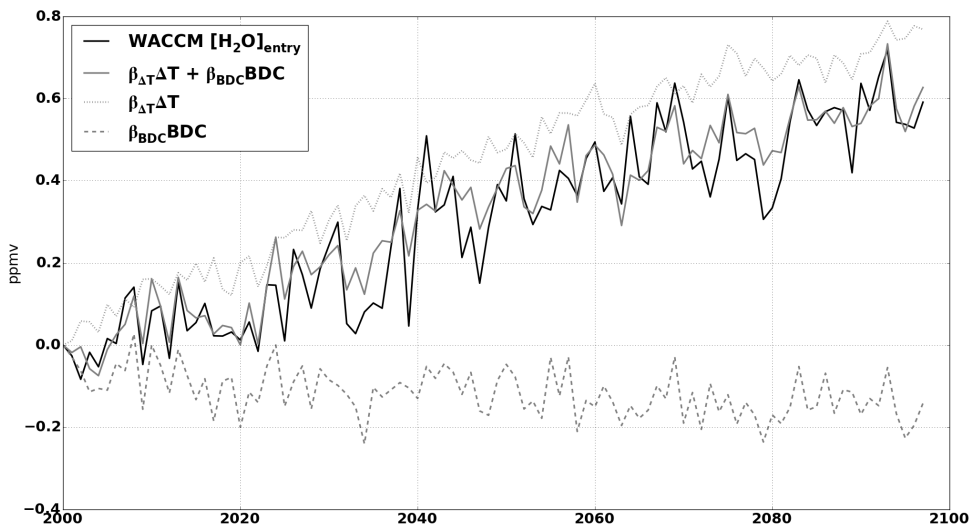

Figure A.11: 21st century annual anomalies of detrended $[H_2O]_{entry}$ from the WACCM (black), and it reconstructed by a multivariate linear regression (gray) using ΔT and BDC (both not shown) annual anomalies as predictors. For this plot, all variables have been detrended by filtering long-term >10 years variations out.